

Gravitino Dark Matter and Cosmological Constraints

Frank Daniel Steffen

Max-Planck-Institut für Physik, Föhringer Ring 6, D-80805 Munich, Germany
E-mail: steffen@mppmu.mpg.de

ABSTRACT: The gravitino is a promising candidate for cold dark matter. We study cosmological constraints on scenarios in which the gravitino is the lightest supersymmetric particle and a charged slepton the next-to-lightest supersymmetric particle (NLSP). We obtain new results for the hadronic nucleosynthesis bounds by computing the 4-body decay of the NLSP slepton into the gravitino, the associated lepton, and a quark–antiquark pair. The bounds from the observed dark matter density are refined by taking into account gravitinos from both late NLSP decays and thermal scattering in the early Universe. We examine the present free-streaming velocity of gravitino dark matter and the limits from observations and simulations of cosmic structures. Assuming that the NLSP sleptons freeze out with a thermal abundance before their decay, we derive new bounds on the slepton and gravitino masses. The implications of the constraints for cosmology and collider phenomenology are discussed and the potential insights from future experiments are outlined. We propose a set of benchmark scenarios with gravitino dark matter and long-lived charged NLSP sleptons and describe prospects for the Large Hadron Collider and the International Linear Collider.

Contents

1. Introduction	1
2. 2-Body Decays of Charged NLSP Sleptons	4
2.1 Lifetime of the Charged Slepton NLSP	4
2.2 Electromagnetic and Hadronic Energy Release from the 2-Body NLSP Decay	5
3. 4-Body Decays of Charged NLSP Sleptons into Hadrons	8
4. Constraints from Primordial Nucleosynthesis	12
4.1 Primordial Nucleosynthesis and Effects of Late NLSP Decays	12
4.2 Upper Limits on the Abundance of Charged Slepton NLSPs before their Decay	17
5. Gravitino Dark Matter from Charged Slepton NLSP Decays	19
5.1 Relic Gravitino Density from NLSP Decays	19
5.2 Free Streaming of Gravitinos and Constraints from Small-Scale Structure	21
6. Bounds on the Gravitino and Charged Slepton NLSP Masses	26
6.1 Estimates of the Abundance of Charged Slepton NLSPs before their Decay	26
6.2 Mass Bounds from the Estimates of the Charged Slepton NLSP Abundance	28
6.3 Mass Bounds for Gravitino Dark Matter Fractions from Slepton NLSP Decays	32
7. Gravitino Dark Matter from Thermal Production	33
7.1 Relic Gravitino Density from Thermal Production in the Early Universe	34
7.2 Free Streaming of Gravitinos from Thermal Production	36
7.3 Upper Limits on the Reheating Temperature	36
8. Prospects for Collider Phenomenology and Cosmology	37
9. Benchmark Scenarios with Gravitino LSP and Stau NLSP	40
10. Conclusions	43

1. Introduction

Supersymmetric extensions of the standard model of particle physics have remarkable properties [1, 2]. In particular, a theory invariant under general coordinate transformations, i.e., supergravity (SUGRA), is obtained once supersymmetry (SUSY) is promoted from a global to a local symmetry.

The gravitino is the gauge field of local SUSY transformations. It is the spin-3/2 superpartner of the graviton and, thus, a singlet with respect to the gauge groups of the standard model. For unbroken SUSY, the gravitino is massless and interacts only gravitationally. Once local SUSY is broken spontaneously, the gravitino acquires a mass and the interactions of the spin-1/2 goldstino (which is the Goldstone spinor associated with the breaking of global SUSY) through the super-Higgs mechanism. The gravitino mass depends strongly on the SUSY-breaking scheme and can range from the eV scale to scales beyond the TeV region [1, 3, 4, 5]. For example, the gravitino mass is typically less than 100 MeV in gauge-mediated SUSY breaking schemes [3] and is expected to be in the GeV to TeV range in gravity-mediated schemes [1]. The gravitino interactions—given by the SUGRA Lagrangian [6, 2]—are suppressed by inverse powers of the (reduced) Planck scale [7]. At energies well above the gravitino mass, these interactions are enhanced as the spin-1/2 goldstino components, which enter through the super-Higgs mechanism, become dominant.

We assume in the following that the gravitino is the lightest supersymmetric particle (LSP) which is stable due to R -parity conservation. If heavier than about 100 keV, the gravitino LSP is a natural candidate for cold dark matter (see [8, 9, 10, 11, 12, 13, 14, 15, 16, 17, 18, 19, 20, 21, 22, 23, 24, 25] and references therein). Gravitino dark matter can originate from both thermal production in the very early Universe [11, 12, 14, 16] and late decays of the next-to-lightest supersymmetric particle (NLSP) [13, 15, 17, 18, 21, 22]. We do not consider other more model-dependent gravitino sources such as inflaton decay [26].

The gravitino LSP scenario is subject to severe cosmological constraints. Upper limits on the reheating temperature after inflation can be obtained since the relic abundance of thermally produced gravitinos cannot exceed the observed abundance of dark matter [11, 15, 16, 23, 25]. Likewise, one can derive upper limits on the gravitino and NLSP masses since the gravitino density from NLSP decays is also bounded from above by the observed dark matter density [15, 22]. Moreover, there are limits on the present free-streaming velocity of the gravitino dark matter from observations and simulations of cosmic structures. Depending on the origin of the gravitinos, these limits can further restrict the allowed range of the gravitino mass and the mass of the NLSP [13, 27].

In addition to the limits from the properties of dark matter, there are also constraints from the observed abundances of the primordial light elements (D, He, Li) [20, 21, 22, 23]. Because of the extremely weak interactions of the gravitino, the NLSP typically has a long lifetime before it decays into the gravitino. If these decays occur during or after primordial nucleosynthesis, the standard model particles emitted in addition to the gravitino can affect the abundance of the primordial light elements. The effects of both electromagnetic and hadronic showers can be important depending on the lifetime of the NLSP (see [28, 29] and references therein). Bounds on the gravitino and NLSP masses can be derived by demanding that the successful predictions of primordial nucleosynthesis be preserved.

Nucleosynthesis constraints have been examined for neutralino NLSP and slepton NLSP scenarios. While most of the existing investigations focus on the effects of electromagnetic energy injection (see [20, 30, 31] and references therein), the bounds from hadronic energy injection can be much more severe [28, 29, 32, 33, 34, 35]. In particular,

the hadronic constraints strongly restrict the mass spectrum in the bino-like neutralino NLSP case [22, 23]. For the slepton NLSP case, the hadronic constraints have also been estimated and found to be much weaker but still significant in much of the parameter space [21, 22, 23].

In this paper we study systematically the cosmological constraints on the gravitino LSP scenario for the case of a charged slepton NLSP. Indeed, the lighter stau $\tilde{\tau}_1$ can appear naturally as the lightest standard model superpartner in frameworks in which the spectrum at low energies is derived from SUGRA predictions at the scale of grand unification. Scenarios with a gravitino LSP and a long-lived charged slepton NLSP are also particularly promising for phenomenology at future colliders [36, 37, 38, 39, 40, 41, 42, 22, 43, 44, 45, 25, 46].

We present new results for the hadronic energy release in late decays of a charged slepton NLSP. We obtain these results from an exact computation of the 4-body decay of the slepton NLSP into the gravitino, the corresponding lepton, and a quark–antiquark pair. The corrections with respect to the previous estimate [21] are indicated explicitly.

Based on our new results, we derive upper limits on the abundance of the charged NLSP slepton before its decay. These limits lead to new bounds on the NLSP and gravitino masses in scenarios in which the NLSP sleptons freeze out with a thermal abundance before their decay. We also refine the bounds from the observed abundance of dark matter by taking into account gravitinos from both slepton NLSP decays [13, 15, 17, 18, 21, 22] and thermal scattering in the early Universe [11, 12, 14, 16]. Upper limits on the reheating temperature after inflation are extracted based on the gauge-invariant treatment of thermal gravitino production [16]. For gravitinos from both NLSP decays and thermal production, we compute the present free-streaming velocity and confront it with limits from observations and simulations of cosmic structures. For each of the considered constraints, we explore associated uncertainties and outline potential refinements from astrophysical observations and experiments at future colliders.

We discuss implications of the cosmological constraints for gravitino dark matter, collider phenomenology, the SUSY breaking scale, and the generation of the baryon asymmetry in thermal leptogenesis [47, 48]. Based on our findings, we propose and examine a set of benchmark scenarios with gravitino dark matter and long-lived charged NLSP sleptons. We consider a wide range of gravitino, slepton NLSP, and gluino masses, and our study is not restricted to a constrained framework such as the constrained minimal supersymmetric extension of the standard model (CMSSM) [20, 23].

The rest of this paper is organized as follows. In Sec. 2 we consider the 2-body decay of the charged slepton NLSP into the gravitino and the associated lepton. This decay mode governs the lifetime of the NLSP and the bounds from late electromagnetic energy injection. In Sec. 3 we present our results on the hadronic 4-body decay of the slepton NLSP. Section 4 reviews the nucleosynthesis constraints for late decaying particles and provides our new upper limits on the abundance of the charged slepton NLSP before its decay. In Sec. 5 we study the relic density and the present free-streaming velocity of gravitinos from NLSP decays and the corresponding bounds. An update of the cosmological constraints on the gravitino and slepton NLSP masses is given in Sec. 6. In Sec. 7 we discuss the thermal production of gravitinos, their present free-streaming velocity, and the bounds

on the reheating temperature after inflation. Section 8 describes the possible interplay between astrophysics and collider phenomenology in view of the cosmological constraints. We summarize the implications for cosmology and collider phenomenology by proposing ten viable benchmark scenarios with gravitino dark matter and a long-lived charged slepton.

2. 2-Body Decays of Charged NLSP Sleptons

In this section we consider the 2-body decay of a charged NLSP slepton into the corresponding lepton and the gravitino LSP. We study the lifetime of the slepton NLSP, which is governed by this decay mode, and discuss the release of electromagnetic and hadronic energy resulting from such 2-body decays in view of the nucleosynthesis constraints.

We concentrate on the scenario where the lighter stau $\tilde{\tau}_1$ is the NLSP, but address also the alternative selectron or smuon NLSP cases. Indeed, the mass spectrum of the superparticles could be such that the masses of the lighter selectron \tilde{e}_1 , the lighter smuon $\tilde{\mu}_1$, and the lighter stau $\tilde{\tau}_1$ are nearly degenerate, $m_{\tilde{\tau}} \approx m_{\tilde{e},\tilde{\mu}}$. Then, the decays of these selectrons, smuons, and staus can be equally important for the constraints from primordial nucleosynthesis. However, if the stau is significantly lighter than its first- and second-generation counterparts, the effects of the selectron and smuon decays on the primordial light elements will be negligible. This results from negligible abundances of selectrons and smuons at the time when the stau NLSP decays into the gravitino LSP; cf. Sec. 6.1.

The two staus are in general a linear combination of $\tilde{\tau}_R$ and $\tilde{\tau}_L$, which are the superpartners of the right-handed and left-handed tau lepton, respectively: $\tilde{\tau}_{1,2} = \cos\theta_\tau\tilde{\tau}_R + \sin\theta_\tau\tilde{\tau}_L$. We focus for simplicity on a purely ‘right-handed’ lighter stau, $\tilde{\tau}_1 = \tilde{\tau}_R$. This is a good approximation at least for small values of $\tan\beta \equiv v_u/v_d$, where $v_{u,d} = \langle H_{u,d}^0 \rangle$ denote the vacuum expectation values of the two neutral Higgs scalar fields of the minimal supersymmetric standard model (MSSM). Then, the neutralino–stau coupling is dominated by the bino coupling. We also assume for simplicity that the lightest neutralino is a pure bino.

2.1 Lifetime of the Charged Slepton NLSP

In the gravitino LSP scenario, the 2-body decay $\tilde{\tau} \rightarrow \tau\tilde{G}$ is the main decay mode of the stau NLSP. Neglecting the τ mass, the SUGRA Lagrangian [6, 2] leads to the following tree-level result for the decay rate

$$\Gamma(\tilde{\tau}_R \rightarrow \tau\tilde{G}) = \frac{m_{\tilde{\tau}}^5}{48\pi m_{\tilde{G}}^2 M_{\text{Pl}}^2} \left(1 - \frac{m_{\tilde{G}}^2}{m_{\tilde{\tau}}^2}\right)^4 \quad (2.1)$$

$$= (6.1 \times 10^3 \text{ s})^{-1} \left(\frac{m_{\tilde{\tau}}}{1 \text{ TeV}}\right)^5 \left(\frac{100 \text{ GeV}}{m_{\tilde{G}}}\right)^2 \left(1 - \frac{m_{\tilde{G}}^2}{m_{\tilde{\tau}}^2}\right)^4, \quad (2.2)$$

which is also valid for any mixture $\tilde{\tau} = \cos\theta_\tau\tilde{\tau}_R + \sin\theta_\tau\tilde{\tau}_L$. To get expression (2.2), we have used the value of the reduced Planck mass $M_{\text{Pl}} = (8\pi G_{\text{N}})^{-1/2} = 2.435 \times 10^{18} \text{ GeV}$ as obtained from macroscopic measurements of Newton’s constant [7] $G_{\text{N}} = 6.709 \times 10^{-39} \text{ GeV}^{-2}$. Thus, the stau NLSP lifetime, $\tau_{\tilde{\tau}} \approx 1/\Gamma(\tilde{\tau}_R \rightarrow \tau\tilde{G})$, is determined by the gravitino mass

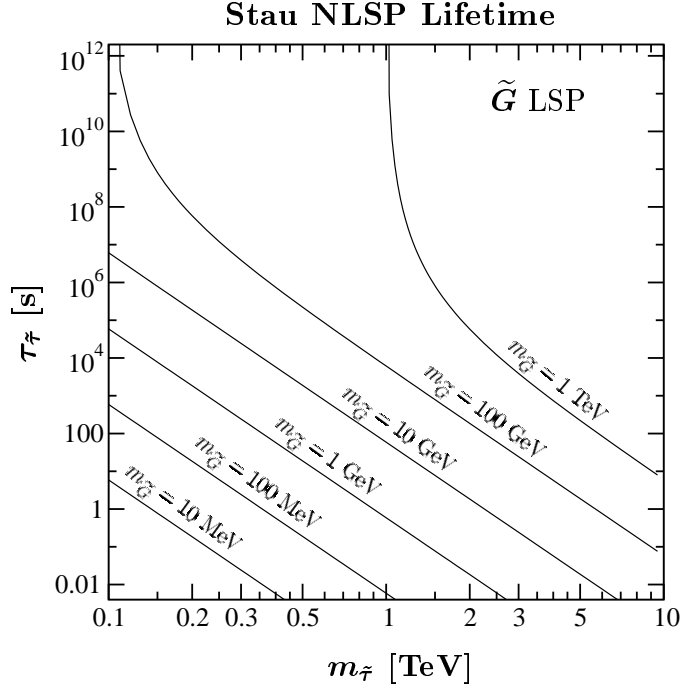


Figure 1: The lifetime of the stau NLSP as a function of its mass $m_{\tilde{\tau}}$ for values of the gravitino mass $m_{\tilde{G}}$ ranging from 10 MeV up to 1 TeV.

$m_{\tilde{G}}$ and the stau NLSP mass $m_{\tilde{\tau}}$. With the replacement $m_{\tilde{\tau}} \rightarrow m_{\tilde{e}, \tilde{\mu}}$, the results for the selectron NLSP and smuon NLSP cases are identical to the one given above.

In Fig. 1 we plot the lifetime of the stau NLSP as a function of its mass $m_{\tilde{\tau}}$ for values of the gravitino mass $m_{\tilde{G}}$ ranging from 10 MeV up to 1 TeV. This figure shows the strong sensitivity of the stau NLSP lifetime on $m_{\tilde{G}}$ and $m_{\tilde{\tau}}$. Indeed, $\tau_{\tilde{\tau}}$ can be in the range from 0.01 s to 10^{12} s and beyond. The contribution from the longitudinal helicity-1/2 (or goldstino) components to the decay rate dominates for $m_{\tilde{\tau}} \gtrsim 3 m_{\tilde{G}}$. For values of $m_{\tilde{\tau}}$ close to $m_{\tilde{G}}$, these contributions become less important and the phase space shrinks so that the stau NLSP lifetime tends to infinity as illustrated for $m_{\tilde{G}} = 100$ GeV and $m_{\tilde{G}} = 1$ TeV.

2.2 Electromagnetic and Hadronic Energy Release from the 2-Body NLSP Decay

Depending on the lifetime $\tau_{\tilde{\tau}}$, the tau emitted in the stau NLSP decay can affect the abundance of the light elements produced in primordial nucleosynthesis. At the time of its decay, the stau NLSP is non-relativistic and can be considered to be at rest with respect to the background. In the NLSP rest frame or comoving frame, the initial energy of the tau (with a mass of $m_{\tau} = 1.777$ GeV) from the 2-body decay is given by

$$E_{\tau} = \frac{m_{\tilde{\tau}}^2 - m_{\tilde{G}}^2 + m_{\tau}^2}{2 m_{\tilde{\tau}}} . \quad (2.3)$$

Accordingly, the emitted tau has a time-dilated lifetime of $\tau_{\tau} = 2.9 \times 10^{-13} (E_{\tau}/m_{\tau})$ s .

If the tau scatters off the background plasma before its decay, the 2-body decay of one stau NLSP gives no hadronic energy release, $\epsilon_{\text{had}}(\tilde{\tau} \rightarrow \tau \tilde{G}) = 0$, but an electromagnetic energy release of $\epsilon_{\text{em}}(\tilde{\tau} \rightarrow \tau \tilde{G}) = E_\tau$, i.e., the full initial tau energy (2.3) ends up in an electromagnetic shower. However, when the temperature of the Universe drops below about 0.5 MeV, which corresponds to a cosmic time of a few seconds, the interaction time of the tau with the background plasma exceeds its time-dilated lifetime even for $E_\tau = \mathcal{O}(1 \text{ TeV})$. One then has to consider the tau decays and the effects of the associated decay products.

In each tau decay, at least one neutrino is emitted. Since neutrinos are only weakly interacting, the effect of their injection is typically subleading [49, 50]. With (basically invisible) energy carried away by neutrinos, the electromagnetic energy release $\epsilon_{\text{em}}(\tilde{\tau} \rightarrow \tau \tilde{G})$ can be reduced down to about one third of the initial tau energy (2.3) [18].

The tau has a sizeable number of decay modes. In addition to neutrinos, one finds that also electrons and unstable particles such as μ , π^\pm , π^0 , K^\pm , and K^0 appear as decay products. For the computation of $\epsilon_{\text{em,had}}(\tilde{\tau} \rightarrow \tau \tilde{G})$, one therefore has to examine not only the interactions of these secondary particles but also the decays of the unstable particles and the interactions of their decay products with the primordial plasma. Depending on the envisaged level of rigor, this can be a tedious task.

Let us here describe the effects of the mesons emitted in the main decay modes of the tau lepton without going into the details. The neutral π^0 meson contributes only to electromagnetic energy injection because it decays purely electromagnetically before interacting with the background plasma. The charged mesons π^\pm and K^\pm also contribute to electromagnetic energy injection. Indeed, their electromagnetic interaction time is significantly shorter than their hadronic one [32]. These mesons thus deposit basically all of their kinetic energy in the electromagnetic cascades when scattering off the background plasma. After these mesons are stopped, they still can induce proton–neutron interconversion processes, which can affect the abundances of the primordial light elements. Also, the neutral K_L^0 mesons, which cannot be stopped electromagnetically, can trigger proton–neutron interconversion processes. At cosmic times of $t \gtrsim 100 \text{ s}$ or, equivalently, temperatures of $T \lesssim 0.1 \text{ MeV}$, however, the emitted π^\pm , K^\pm , and K^0 mesons typically decay before interacting hadronically [29]. Accordingly, the hadronic effects of the mesons from the tau decays can only be relevant for stau NLSP decays at temperatures of $0.1 \text{ MeV} \lesssim T \lesssim 0.5 \text{ MeV}$, which corresponds to cosmic times of $3 \text{ s} \lesssim t \lesssim 100 \text{ s}$.

In this paper we will concentrate on decays at late times of $t \gtrsim 100 \text{ s}$, where the hadronic effects of the emitted mesons can be neglected so that $\epsilon_{\text{had}}(\tilde{\tau} \rightarrow \tau \tilde{G}) = 0$. Then, the 4-body decay of the stau NLSP into the gravitino, the tau, and a quark–antiquark pair governs the constraints from late hadronic energy injection. The hadronic energy release from this 4-body decay will be computed in the next section.

Upper limits on electromagnetic energy release become most severe at cosmic times of $10^7 \text{ s} \lesssim t \lesssim 10^{12} \text{ s}$, as will be shown explicitly in Sec. 4.2. The resulting constraints are governed by the 2-body decay $\tilde{\tau} \rightarrow \tau \tilde{G}$ and were studied for $\epsilon_{\text{em}}(\tilde{\tau} \rightarrow \tau \tilde{G}) = 0.5 E_\tau$ in [18, 21, 22, 23] and for $\epsilon_{\text{em}}(\tilde{\tau} \rightarrow \tau \tilde{G}) = 0.3 E_\tau$ in [20]. The true value of $\epsilon_{\text{em}}(\tilde{\tau} \rightarrow \tau \tilde{G})$ can deviate from these values depending on the lifetime of the stau NLSP. We will explore

Electromagnetic Energy Release per $\tilde{\tau}$ NLSP Decay

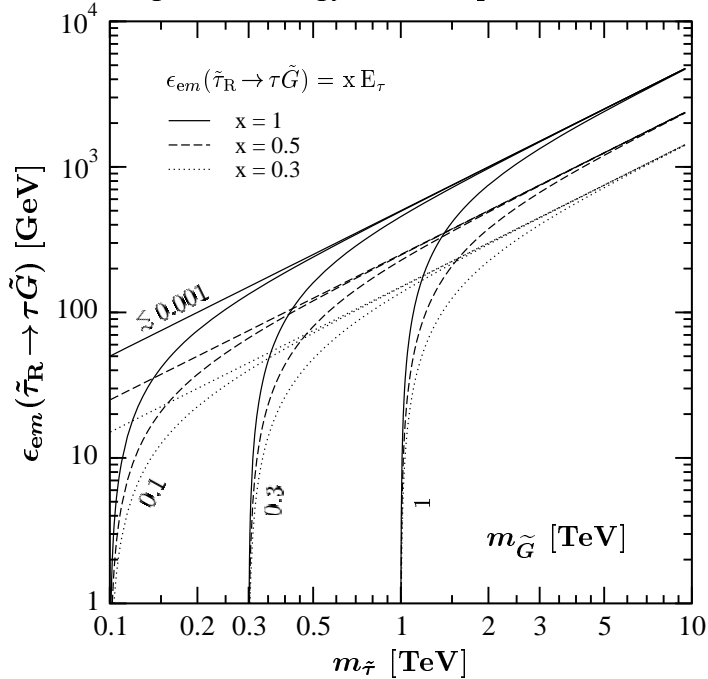


Figure 2: The electromagnetic energy release from the 2-body decay of a single stau NLSP as a function of $m_{\tilde{\tau}}$ for $m_{\tilde{G}} \lesssim 1$ GeV and $m_{\tilde{G}} = 100$ GeV, 300 GeV, and 1 TeV. The solid, dashed, and dotted lines are obtained with $\epsilon_{\text{em}}(\tilde{\tau} \rightarrow \tau \tilde{G}) = E_{\tau}$, $0.5 E_{\tau}$, and $0.3 E_{\tau}$, respectively.

the electromagnetic constraints again only for representative values:

$$\epsilon_{\text{em}}(\tilde{\tau} \rightarrow \tau \tilde{G}) = x E_{\tau} \quad \text{with} \quad x = 0.3, 0.5, 1. \quad (2.4)$$

In Fig. 2 we show $\epsilon_{\text{em}}(\tilde{\tau} \rightarrow \tau \tilde{G}) = E_{\tau}$ (solid lines), $0.5 E_{\tau}$ (dashed lines), and $0.3 E_{\tau}$ (dotted lines) as a function of $m_{\tilde{\tau}}$ for $m_{\tilde{G}} \lesssim 1$ GeV and $m_{\tilde{G}} = 100$ GeV, 300 GeV, and 1 TeV. Note that the true electromagnetic energy release is always below $\epsilon_{\text{em}}(\tilde{\tau} \rightarrow \tau \tilde{G}) = E_{\tau}$ for a stau NLSP that decays at a cosmic time of $100 \text{ s} \lesssim t \lesssim 10^{12} \text{ s}$. Accordingly, the constraints obtained for $\epsilon_{\text{em}}(\tilde{\tau} \rightarrow \tau \tilde{G}) = E_{\tau}$ are overly restrictive for stau NLSP scenarios.

In the selectron NLSP case, the electromagnetic energy injection is governed by the 2-body decay $\tilde{e} \rightarrow e \tilde{G}$ in which a (stable) electron is emitted with an energy of $E_e = (m_{\tilde{e}}^2 - m_{\tilde{G}}^2 + m_e^2)/(2m_{\tilde{e}})$. Accordingly, an electromagnetic and hadronic energy of respectively $\epsilon_{\text{em}}(\tilde{e} \rightarrow e \tilde{G}) \simeq E_e$ and $\epsilon_{\text{had}}(\tilde{e} \rightarrow e \tilde{G}) \simeq 0$ is released in the 2-body decay of one selectron NLSP. For the case of the selectron NLSP, the electromagnetic energy release is described by the same solid curves in Fig. 2 since the differences resulting from the different lepton masses are negligible.

In the smuon NLSP case, the 2-body decay $\tilde{\mu} \rightarrow \mu \tilde{G}$ injects a muon with an energy of $E_{\mu} = (m_{\tilde{\mu}}^2 - m_{\tilde{G}}^2 + m_{\mu}^2)/(2m_{\tilde{\mu}})$ into the primordial plasma. This muon has a time-dilated lifetime of $2.2 \times 10^{-6} (E_{\mu}/m_{\mu}) \text{ s}$. As long as the temperature of the Universe is above about 0.3 keV, which corresponds to cosmic times $t \lesssim 1.5 \times 10^4 \text{ s}$, this muon initiates an electromagnetic cascade so that $\epsilon_{\text{em}}(\tilde{\mu} \rightarrow \mu \tilde{G}) \simeq E_{\mu}$ while $\epsilon_{\text{had}}(\tilde{\mu} \rightarrow \mu \tilde{G}) \simeq 0$. If the muon

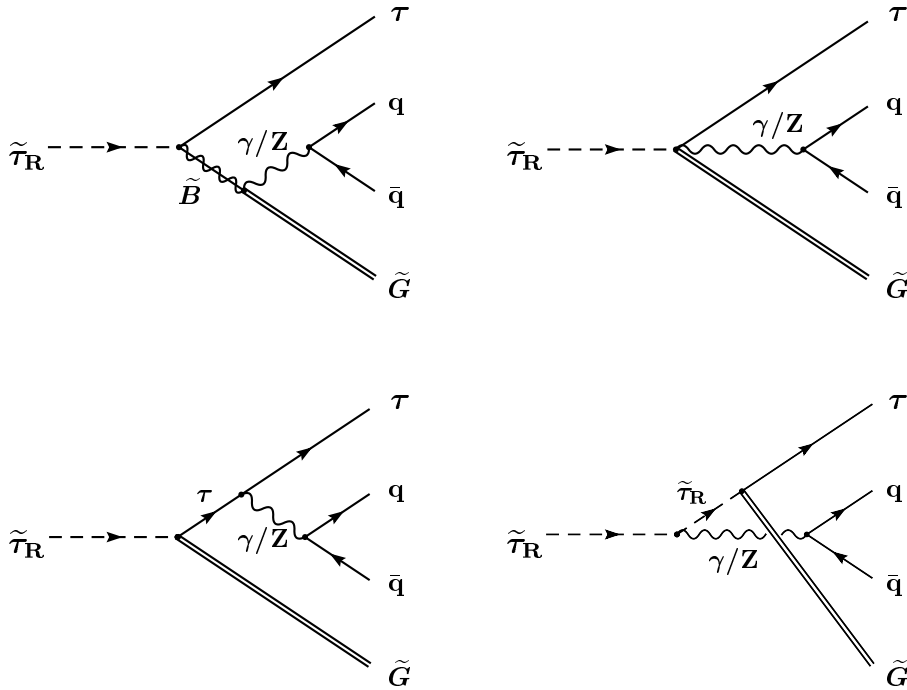


Figure 3: The 4-body NLSP decay $\tilde{\tau}_R \rightarrow \tau \tilde{G} q \bar{q}$

is emitted at later times or, equivalently, lower temperatures, it decays via $\mu \rightarrow e \nu_e \nu_\mu$ before interacting with the background plasma. Accordingly, the electromagnetic energy release is reduced to about $\epsilon_{\text{em}}(\tilde{\mu} \rightarrow \mu \tilde{G}) \approx 0.3 E_\mu$ for smuon NLSP decays at $t \gtrsim 1.5 \times 10^4$ s. The hadronic energy release remains at $\epsilon_{\text{had}}(\tilde{\mu} \rightarrow \mu \tilde{G}) \simeq 0$. For such late decays, the electromagnetic energy release as a function of the smuon mass can be read from the dotted curves in Fig. 2 since the effect of the different lepton masses is again negligible.

3. 4-Body Decays of Charged NLSP Sleptons into Hadrons

In this section we compute the 4-body decay of a charged NLSP slepton into the corresponding lepton, the gravitino LSP, and a quark–antiquark pair. We present our results for the branching ratio of this decay mode, the associated hadronic energy spectrum, and the resulting hadronic energy release per slepton NLSP decay. We compare the results from our exact treatment of the 4-body decay with the previous estimate derived in Ref. [21].

We compute the leading contribution to the 4-body decay $\tilde{l}_R \rightarrow l \tilde{G} q \bar{q}$. To be specific, we discuss our results for the scenario in which the $\tilde{\tau}_R$ is the NLSP. Nevertheless, the results given in this section can be applied directly to \tilde{e}_R or $\tilde{\mu}_R$ NLSP scenarios by performing obvious substitutions such as $m_{\tilde{\tau}} \rightarrow m_{\tilde{e}, \tilde{\mu}}$.

The Feynman diagrams of the leading contributions to $\tilde{\tau}_R \rightarrow \tau \tilde{G} q \bar{q}$ are shown in Fig. 3. The couplings of the gravitino to the stau, tau, bino (\tilde{B}), and the electroweak gauge bosons are given by the SUGRA Lagrangian [6, 2]. In our computation of the squared matrix element, the exchange of virtual photons (γ^*) and virtual Z bosons (Z^*) is included. The

width of the Z boson is taken into account by using the Breit–Wigner form of the Z-boson propagator. We neglect the lepton mass. We also assume that the lightest neutralino is a pure bino as already mentioned. The other neutralinos and the squarks are assumed to be much heavier than the stau NLSP and the bino. Depending on the invariant mass of the quark–antiquark pair $m_{q\bar{q}}$, up to five quark flavors are considered. The contributions from $t\bar{t}$ -final states, which can appear for $m_{q\bar{q}} \gtrsim 350$ GeV, are subleading. The masses of the quarks are taken into account only in the phase space integration. Only quark–antiquark pairs with an invariant mass of at least $m_{q\bar{q}}^{\text{cut}} = 2$ GeV, i.e. the mass of a nucleon pair, are considered. This choice for the cut on $m_{q\bar{q}}$ will be motivated below. Performing the phase space integrations numerically, we obtain the results presented in Figs. 4 to 8 below.

The branching ratio of the 4-body decay $\tilde{\tau}_R \rightarrow \tau \tilde{G} q \bar{q}$ with $m_{q\bar{q}} \geq m_{q\bar{q}}^{\text{cut}}$ is given by

$$\text{BR}(\tilde{\tau}_R \rightarrow \tau \tilde{G} q \bar{q}; m_{q\bar{q}}^{\text{cut}}) \equiv \frac{\Gamma(\tilde{\tau}_R \rightarrow \tau \tilde{G} q \bar{q}; m_{q\bar{q}}^{\text{cut}})}{\Gamma_{\tilde{\tau}_R}^{\text{total}}}, \quad (3.1)$$

where the total width of the stau NLSP $\Gamma_{\tilde{\tau}_R}^{\text{total}}$ is dominated by the 2-body decay

$$\Gamma_{\tilde{\tau}}^{\text{total}} \simeq \Gamma(\tilde{\tau}_R \rightarrow \tau \tilde{G}). \quad (3.2)$$

The partial width of the 4-body decay with a cut on the invariant mass $m_{q\bar{q}}$ is defined as

$$\Gamma(\tilde{\tau}_R \rightarrow \tau \tilde{G} q \bar{q}; m_{q\bar{q}}^{\text{cut}}) \equiv \int_{m_{q\bar{q}}^{\text{cut}}}^{m_{\tilde{\tau}} - m_{\tilde{G}} - m_{\tau}} dm_{q\bar{q}} \frac{d\Gamma(\tilde{\tau}_R \rightarrow \tau \tilde{G} q \bar{q})}{dm_{q\bar{q}}}. \quad (3.3)$$

In Fig. 4 the branching ratio of the decay $\tilde{\tau}_R \rightarrow \tau \tilde{G} q \bar{q}$ is shown as a function of $m_{\tilde{\tau}}$ for $m_{\tilde{G}} \lesssim 1$ GeV (left) and $m_{\tilde{G}} = 100$ GeV (right). The curves are obtained with $m_{q\bar{q}}^{\text{cut}} = 2$ GeV and a bino mass of $m_{\tilde{B}} = 1.1 m_{\tilde{\tau}}$. The contributions from pure γ^* and pure Z^* exchange are indicated by the dashed and dotted lines, respectively. The solid lines present the full results in which also the γ^* – Z^* interference is taken into account. For $m_{\tilde{\tau}} \rightarrow m_{\tilde{G}}$, the phase space shrinks so that the considered branching ratio tends to zero as illustrated for $m_{\tilde{G}} = 100$ GeV.

In Fig. 5 we show the branching ratio of $\tilde{\tau}_R \rightarrow \tau \tilde{G} q \bar{q}$ as a function of $m_{\tilde{\tau}}$ for values of $m_{\tilde{G}}$ up to 1 TeV, where, again, $m_{q\bar{q}}^{\text{cut}} = 2$ GeV and $m_{\tilde{B}} = 1.1 m_{\tilde{\tau}}$. The full results are given by the solid lines and the respective contributions from pure Z^* exchange by the dotted lines.

In previous studies, the hadronic branching ratio was estimated from a real Z boson in the final state and its hadronic branching fraction [21]. These estimates (obtained in the zero-width approximation) differ very little from the dotted lines shown in Figs. 4 and 5. In other words, the hadronic branching ratio was significantly underestimated in Refs. [21, 22, 23] towards smaller values of $m_{\tilde{\tau}}$, where the photon exchange gives the dominant contribution.

The energy spectrum of the emitted hadrons is also important for the investigation of the nucleosynthesis constraints. As mentioned in the previous section, we concentrate on decays at cosmic times of $t \gtrsim 100$ s, where the hadronic effects of the mesons from the tau

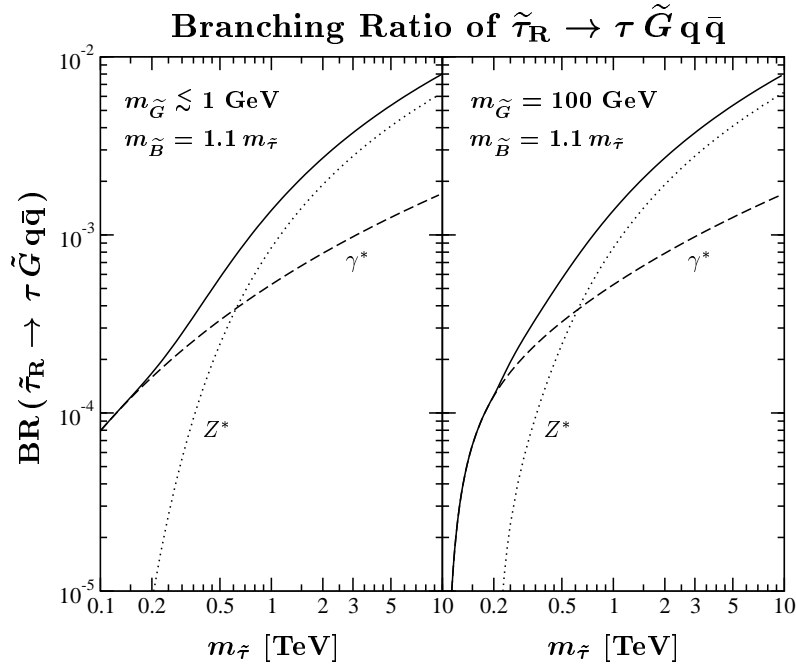


Figure 4: The branching ratio of the 4-body decay $\tilde{\tau}_R \rightarrow \tau \tilde{G} q \bar{q}$ as a function of $m_{\tilde{\tau}}$ for $m_{\tilde{G}} \lesssim 1$ GeV (left) and $m_{\tilde{G}} = 100$ GeV (right). The solid lines give the full results including γ^* - Z^* interference. The dashed and dotted lines show the contributions from pure γ^* and pure Z^* exchange, respectively. The curves are obtained with $m_{q\bar{q}}^{\text{cut}} = 2$ GeV and a bino mass of $m_{\tilde{B}} = 1.1 m_{\tilde{\tau}}$. For comparison, the previous estimates of the branching ratio inferred from a real Z boson (i.e., in the zero width approximation) alone [21] coincide basically with the dotted lines.

decays can be neglected. Thus, the initial hadronic energy is determined by the invariant mass $m_{q\bar{q}}$ of the quark–antiquark pair emitted in the considered 4-body decay.

In Fig. 6 the energy spectrum of the quark–antiquark pair normalized to the partial width of the 4-body decay,

$$\frac{1}{\Gamma(\tilde{\tau}_R \rightarrow \tau \tilde{G} q \bar{q}; m_{q\bar{q}}^{\text{cut}} = 2 \text{ GeV})} \frac{d\Gamma(\tilde{\tau}_R \rightarrow \tau \tilde{G} q \bar{q})}{dm_{q\bar{q}}}, \quad (3.4)$$

is shown for $(m_{\tilde{G}}, m_{\tilde{\tau}}) = (1 \text{ GeV}, 1 \text{ TeV})$, $(1 \text{ GeV}, 0.2 \text{ TeV})$, $(100 \text{ GeV}, 0.2 \text{ TeV})$, and $(10 \text{ GeV}, 0.1 \text{ TeV})$ by the solid, dashed, dotted, and dash-dotted curves, respectively, where $m_{\tilde{B}} = 1.1 m_{\tilde{\tau}}$. The solid, dashed, and dotted curves illustrate that the importance of the Z-boson resonance at $m_{q\bar{q}} = M_Z$ grows with increasing mass difference $\Delta m \equiv m_{\tilde{\tau}} - m_{\tilde{G}}$. For a mass difference Δm less than the Z-boson mass, however, the Z boson cannot become resonant and the photon exchange dominates as illustrated by the dash-dotted curve. The kinks at $m_{q\bar{q}} \simeq 4$ GeV and 10 GeV mark the threshold energies for the production of $c\bar{c}$ and $b\bar{b}$ pairs respectively.

Having computed the initial energy spectrum of the quark–antiquark pairs for given values of $m_{\tilde{\tau}}$ and $m_{\tilde{G}}$, one should consider the fragmentation of the initial quark–antiquark pairs into hadrons. The resulting meson and nucleon spectra should then be taken into account when computing the abundances of the primordial light elements; cf. [29, 51]. We

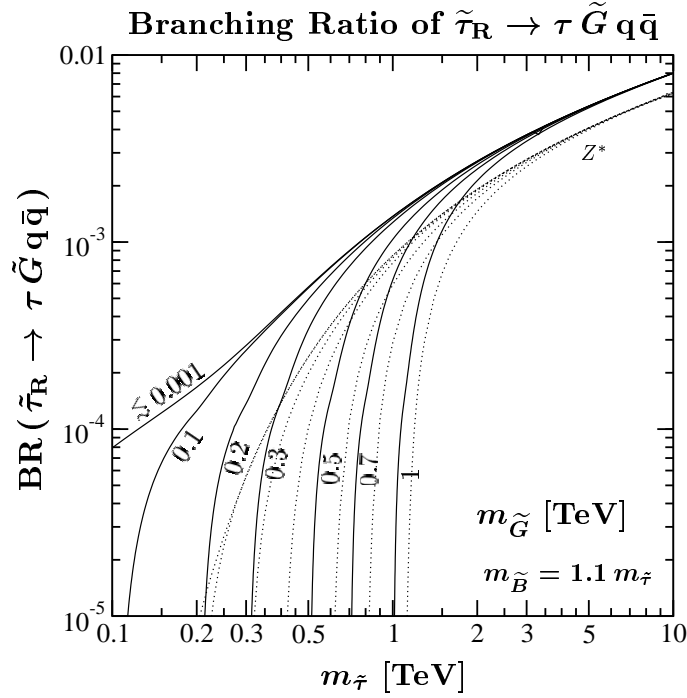


Figure 5: The branching ratio of the 4-body decay $\tilde{\tau}_R \rightarrow \tau \tilde{G} q \bar{q}$ as a function of $m_{\tilde{\tau}}$ for $m_{\tilde{G}} \lesssim 1$ GeV and $m_{\tilde{G}} = 0.1, 0.2, 0.3, 0.5, 0.7,$ and 1 TeV (from the left to the right). The solid lines present the full results and the dotted lines the contributions from pure Z^* exchange for comparison with the previous estimates. The curves are obtained with $m_{q\bar{q}}^{\text{cut}} = 2$ GeV and a bino mass of $m_{\tilde{B}} = 1.1 m_{\tilde{\tau}}$.

will not follow this procedure. Instead, we will adopt the limits on the *initial* hadronic energy release from [28, 29], where the hadronization of primary partons is already taken into account. These limits are most severe for decays at cosmic times $t \gtrsim 100$ s. For such late decays, the emitted nucleons govern the constraints since—as already mentioned—the mesons typically decay before interacting with the background nuclei. We therefore consider only quark–antiquark pairs with an invariant mass greater than the mass of a pair of nucleons, $m_{q\bar{q}}^{\text{cut}} = 2$ GeV.

Our study of the hadronic nucleosynthesis constraints is based on the computation of the average initial hadronic energy release in the 4-body decay of a single stau NLSP

$$\epsilon_{\text{had}}(\tilde{\tau}_R \rightarrow \tau \tilde{G} q \bar{q}) \equiv \frac{1}{\Gamma_{\tilde{\tau}}^{\text{total}}} \int_{m_{q\bar{q}}^{\text{cut}}}^{m_{\tilde{\tau}} - m_{\tilde{G}} - m_{\tau}} dm_{q\bar{q}} m_{q\bar{q}} \frac{d\Gamma(\tilde{\tau}_R \rightarrow \tau \tilde{G} q \bar{q})}{dm_{q\bar{q}}} . \quad (3.5)$$

In Fig. 7 this quantity is shown as a function of $m_{\tilde{\tau}}$ for $m_{\tilde{G}} \lesssim 1$ GeV (left) and $m_{\tilde{G}} = 100$ GeV (right), where $m_{q\bar{q}}^{\text{cut}} = 2$ GeV and $m_{\tilde{B}} = 1.1 m_{\tilde{\tau}}$. The solid lines present the full results and the dashed and dotted lines the contributions from pure γ^* and pure Z^* exchange, respectively. In Fig. 8, the solid lines show the full results for gravitino masses up to 1 TeV. In addition, the dotted lines show the curves obtained with the estimate from Ref. [21]

$$\epsilon_{\text{had}}(\text{FST '04}) \equiv \frac{1}{3} (m_{\tilde{\tau}} - m_{\tilde{G}}) \text{BR}(\tilde{\tau}_R \rightarrow \tau \tilde{G} Z) \text{BR}(Z \rightarrow q \bar{q}) , \quad (3.6)$$

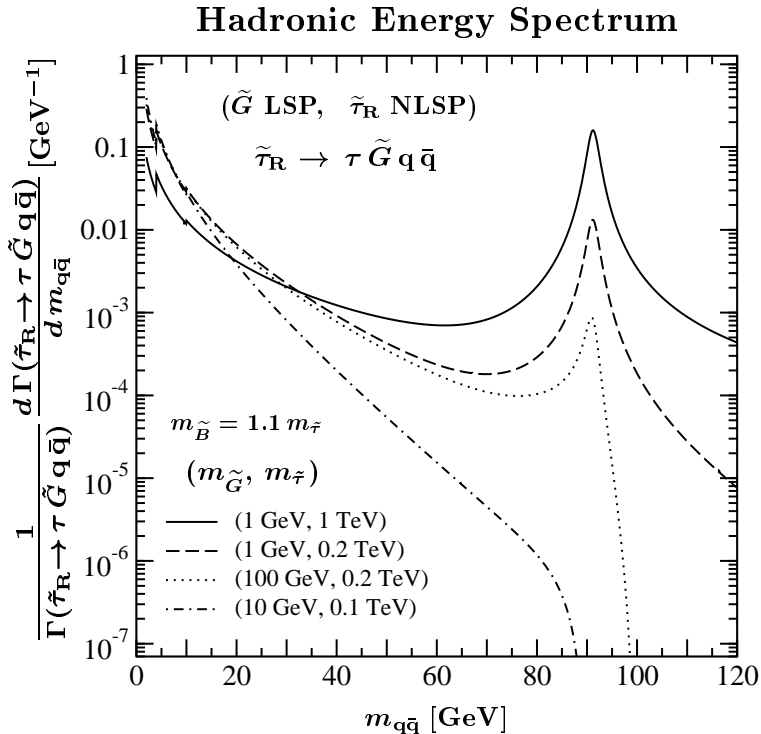


Figure 6: The normalized energy spectrum of quark–antiquark pairs emitted in the 4-body decay $\tilde{\tau}_R \rightarrow \tau \tilde{G} q \bar{q}$ with an invariant mass $m_{q\bar{q}}$. The solid, dashed, dotted, and dash-dotted curves are obtained respectively for $(m_{\tilde{G}}, m_{\tilde{\tau}}) = (1 \text{ GeV}, 1 \text{ TeV}), (1 \text{ GeV}, 0.2 \text{ TeV}), (100 \text{ GeV}, 0.2 \text{ TeV}),$ and $(10 \text{ GeV}, 0.1 \text{ TeV})$, where $m_{\tilde{B}} = 1.1 m_{\tilde{\tau}}$.

where the energy of the quark–antiquark pair was approximated as $(m_{\tilde{\tau}} - m_{\tilde{G}})/3$ and only Z-boson exchange in the zero-width approximation was taken into account. From the comparison, we find that the hadronic energy release has been underestimated towards smaller values of $m_{\tilde{\tau}}$ due to the missing contribution from photon exchange and overestimated for $m_{\tilde{\tau}} \gg m_{\tilde{G}}$ due to the monochromatic approximation of the energy of the quark–antiquark pair. Accordingly, one has to update the hadronic constraints inferred from the estimate (3.6) such as the ones given in [21, 22, 23].

4. Constraints from Primordial Nucleosynthesis

In this section we review the nucleosynthesis constraints on hadronic and electromagnetic energy release from late NLSP decays. We use these constraints to derive upper limits on the abundance of charged slepton NLSPs before their decay.

4.1 Primordial Nucleosynthesis and Effects of Late NLSP Decays

Primordial nucleosynthesis, or big-bang nucleosynthesis (BBN), is one of the cornerstones of modern cosmology. With the observed abundance of D and ^4He in the Universe, the standard BBN scenario provides an estimation of the baryon-to-photon ratio, $\eta \equiv n_B/n_\gamma$, which agrees with that inferred from studies of the cosmic microwave background (CMB).

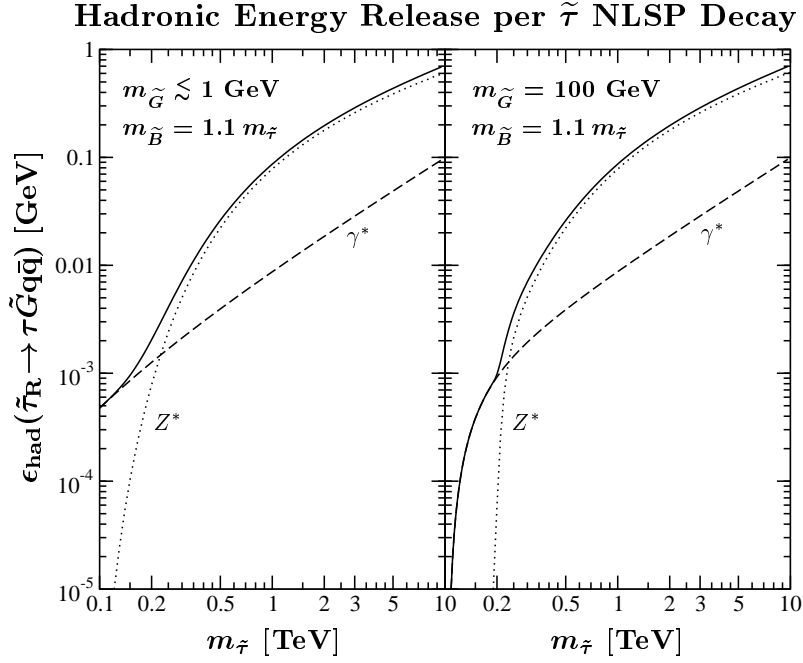


Figure 7: The average hadronic energy release from the 4-body decay of a single stau NLSP as a function of $m_{\tilde{\tau}}$ for $m_{\tilde{G}} \lesssim 1$ GeV (left) and $m_{\tilde{G}} = 100$ GeV (right), where $m_{\tilde{q}\tilde{q}}^{\text{cut}} = 2$ GeV and $m_{\tilde{B}} = 1.1 m_{\tilde{\tau}}$. The solid lines show the full results, and the dashed and dotted lines the contributions from pure γ^* and pure Z^* exchange, respectively.

As mentioned already in the Introduction, this concordance imposes constraints on the considered gravitino LSP scenario since the electromagnetic and hadronic energy released in late NLSP decays can modify the standard BBN scenario substantially.

The dominant mechanism affecting the standard BBN scenario depends on the time t at which the electromagnetic or hadronic energy is injected. In this study we use the sudden decay approximation by assuming that the release of electromagnetic and hadronic energy from the NLSP decay occurs when the cosmic time t equals the NLSP lifetime τ_{NLSP} . For $1 \text{ s} \lesssim \tau_{\text{NLSP}} \lesssim 100 \text{ s}$, energetic hadrons are stopped efficiently through electromagnetic interactions so that the direct destruction of light elements is subdominant. The presence of additional slow hadrons can still change the ratio of protons to neutrons through interconversion processes and thus affect the abundance of the light elements. For $100 \text{ s} \lesssim \tau_{\text{NLSP}} \lesssim 10^7 \text{ s}$, energetic hadrons and, in particular, neutrons cannot be slowed down significantly. Accordingly, they can reprocess efficiently the produced light elements through hadro-dissociation processes. The effect of electromagnetic energy release is negligible for $\tau_{\text{NLSP}} \lesssim 10^4 \text{ s}$ as the interaction with the background particles thermalizes quickly any high-energy photons or leptons emitted in the NLSP decay. Towards later times, electromagnetic energy release becomes important. For $10^7 \text{ s} \lesssim \tau_{\text{NLSP}} \lesssim 10^{12} \text{ s}$, the reprocessing of light elements through energetic electromagnetic showers, i.e., photo-dissociation, can become more significant than hadro-dissociation. (For details, see [32, 29] and references therein.)

Hadronic Energy Release per $\tilde{\tau}$ NLSP Decay

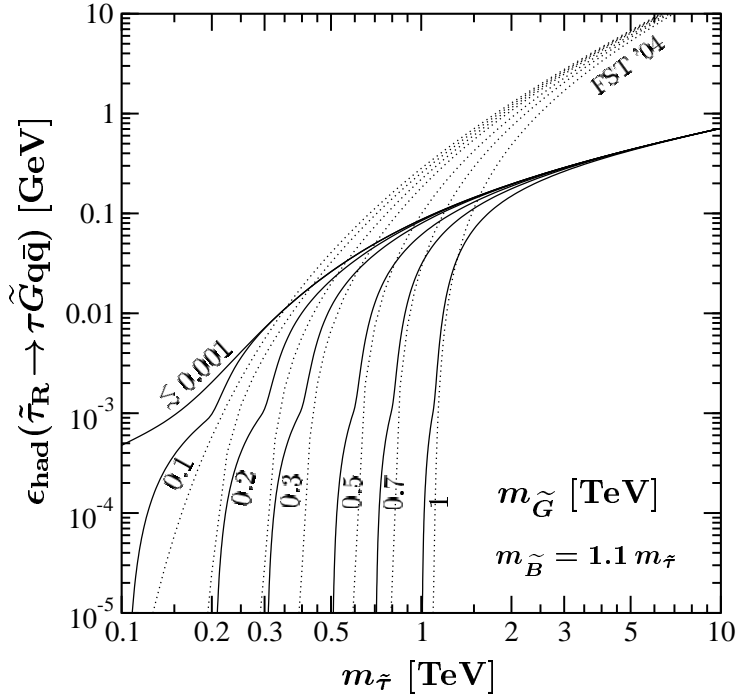


Figure 8: The average hadronic energy release from the 4-body decay of a single stau NLSP as a function of $m_{\tilde{\tau}}$ for $m_{\tilde{G}} = 0.1, 0.2, 0.3, 0.5, 0.7,$ and 1 TeV (solid lines from the left to the right), where $m_{\tilde{q}\tilde{q}}^{\text{cut}} = 2$ GeV and $m_{\tilde{B}} = 1.1 m_{\tilde{\tau}}$. The corresponding previous estimates from [21] are indicated by the dotted lines (FST '04).

The constraints on electromagnetic and hadronic energy release can be quantified conveniently in terms of upper bounds on the quantities

$$\xi_{\text{em,had}} \equiv \epsilon_{\text{em,had}} Y_{\text{NLSP}} . \quad (4.1)$$

Here $\epsilon_{\text{em,had}}$ is the (average) electromagnetic/hadronic energy emitted in a single NLSP decay studied for charged slepton NLSP scenarios in the previous sections. The NLSP yield prior to decay Y_{NLSP} is obtained by dividing the NLSP number density n_{NLSP} prior to decay with the total entropy density of the Universe s :

$$Y_{\text{NLSP}} \equiv \frac{n_{\text{NLSP}}}{s} . \quad (4.2)$$

In this way, one scales out the effect of the expansion of the Universe on the NLSP abundance.

We concentrate on the bounds from the primordial abundances of D and ^4He as they are the most reliable ones. The bounds from ^3He , ^6Li , and ^7Li could be even more severe. However, the observed abundances of these elements are still subject to serious systematic uncertainties.

We work with the recent numerical constraints on electromagnetic and hadronic energy release given in Refs. [28, 29]. These constraints were extracted with the following

observational values of the light element abundances (1σ error):

$$(n_{\text{D}}/n_{\text{H}})_{\text{mean}} \equiv (2.78_{-0.38}^{+0.44}) \times 10^{-5} , \quad (4.3)$$

$$(n_{\text{D}}/n_{\text{H}})_{\text{high}} \equiv (3.98_{-0.67}^{+0.59}) \times 10^{-5} , \quad (4.4)$$

$$Y_{\text{p}}(\text{FO}) = 0.238 \pm (0.002)_{\text{stat}} \pm (0.005)_{\text{syst}} , \quad (4.5)$$

$$Y_{\text{p}}(\text{IT}) = 0.242 \pm (0.002)_{\text{stat}} [\pm(0.005)_{\text{syst}}] . \quad (4.6)$$

Here n_{X} denotes the primordial number density of element X and Y_{p} the primordial value of the mass fraction of ^4He . Observe that two values for $n_{\text{D}}/n_{\text{H}}$ were considered. The one given in (4.3) corresponds to the mean of the existing observations and the other given in (4.4) to the highest value among these observations. The latter of these was used to derive a conservative constraint; cf. Sec. IIA of Ref. [29] and references therein. For Y_{p} , the values from the analysis of Fields and Olive (FO) [53] and from the one of Izotov and Thuan (IT) [54] were used due to the sizeable difference.

We also consider the recent numerical constraints on electromagnetic energy release extracted from more conservative observational bounds on the light element abundances [31]

$$1.3 \times 10^{-5} < n_{\text{D}}/n_{\text{H}} < 5.3 \times 10^{-5} \quad (4.7)$$

$$0.227 < Y_{\text{p}} (< 0.249) . \quad (4.8)$$

For $n_{\text{D}}/n_{\text{H}}$, the upper limit is the 2σ upper limit to the highest value reliably observed. The lower limit is adopted from the observed present abundance in the interstellar medium as galactic processes can only destroy deuterium. For the ^4He abundance, the range is obtained from the analysis of Fields and Olive [53] by taking the 2σ range with errors added in quadrature.

In Fig. 9 we show the numerically obtained upper limits on hadronic and electromagnetic energy release as a function of the NLSP lifetime τ_{NLSP} . The upper part of the figure shows exclusion limits on hadronic energy release $\xi_{\text{had}} \equiv \epsilon_{\text{had}} Y_{\text{NLSP}}$ taken from Fig. 39 of Ref. [29]. The solid (black), dashed (red), dotted (blue), and thin dash-dotted (yellow) lines represent the limits inferred from the observational bounds (4.3), (4.5), (4.6), and (4.4), respectively. These limits were obtained at the 95% confidence level (CL) with a baryon asymmetry of $\eta = (6.1 \pm 0.3) \times 10^{-10}$ by considering a particle of lifetime τ_{NLSP} and mass 1 TeV decaying with a hadronic branching ratio of $B_{\text{had}} = 1$. Note that these limits were found to be rather insensitive to the mass of the decaying particle. The lower part of Fig. 9 shows exclusion limits on electromagnetic energy release $\xi_{\text{em}} \equiv \epsilon_{\text{em}} Y_{\text{NLSP}}$. The solid (black), dashed (red), and dotted (blue) lines are inferred respectively from the observational bounds (4.3), (4.5), and (4.6). These curves are taken from Fig. 42 of Ref. [29]. They indicate the limits at the 95% CL obtained with $\eta = (6.1 \pm 0.3) \times 10^{-10}$ for a particle of lifetime τ_{NLSP} and mass 1 TeV decaying purely electromagnetically, $B_{\text{em}} = 1$. In addition, the exclusion limits on ξ_{em} from the more conservative observational bounds (4.7) and (4.8) are indicated by the thin dash-dotted (yellow) and dotted (yellow) lines, respectively. Accounting for the different normalizations, we adapt these curves (obtained with $\eta = 6 \times 10^{-10}$) from Figs. 6 and 7 of Ref. [31].

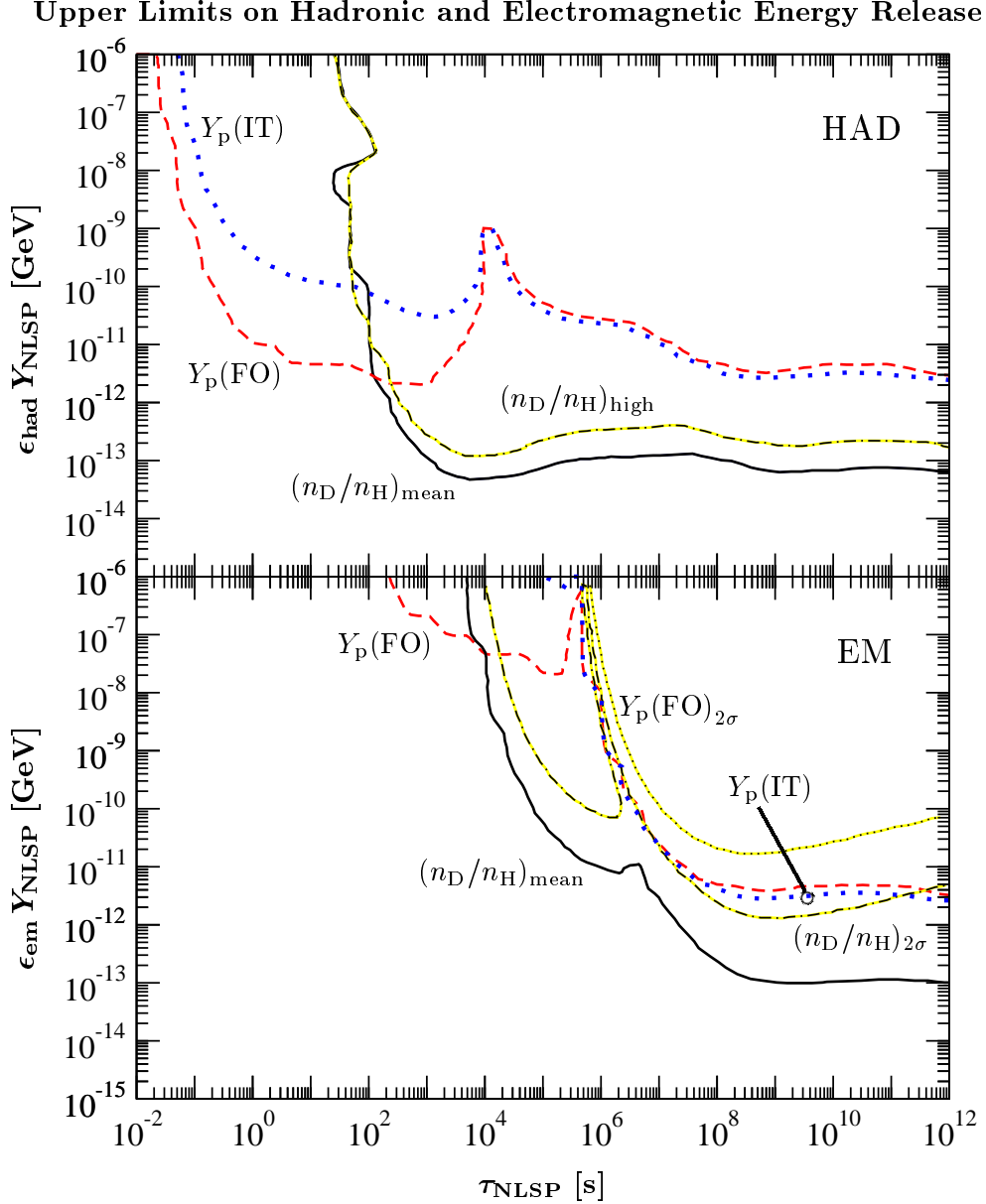


Figure 9: Upper limits on hadronic and electromagnetic energy release from NLSP decays as a function of the NLSP lifetime τ_{NLSP} . The upper plot shows the bounds on $\epsilon_{\text{had}} Y_{\text{NLSP}}$ adapted from Fig. 39 of Ref. [29] and the lower plot the bounds on $\epsilon_{\text{em}} Y_{\text{NLSP}}$ adapted from Fig. 42 of Ref. [29] and Figs. 6 and 7 of Ref. [31]. The solid (black), dashed (red), and dotted (blue) lines result from the observational constraints (4.3), (4.5), and (4.6), respectively. The thin dash-dotted (yellow) lines in the upper and lower plot are obtained from (4.4) and (4.7), respectively. The thin dotted (yellow) curve represents the limit from (4.8).

The upper part of Fig. 9 shows that the limits on hadronic energy release become most severe for $\tau_{\text{NLSP}} \gtrsim 100\text{s}$, where hadro-dissociation processes govern the constraints. As mentioned in the previous sections, we concentrate on this region. We do not consider the

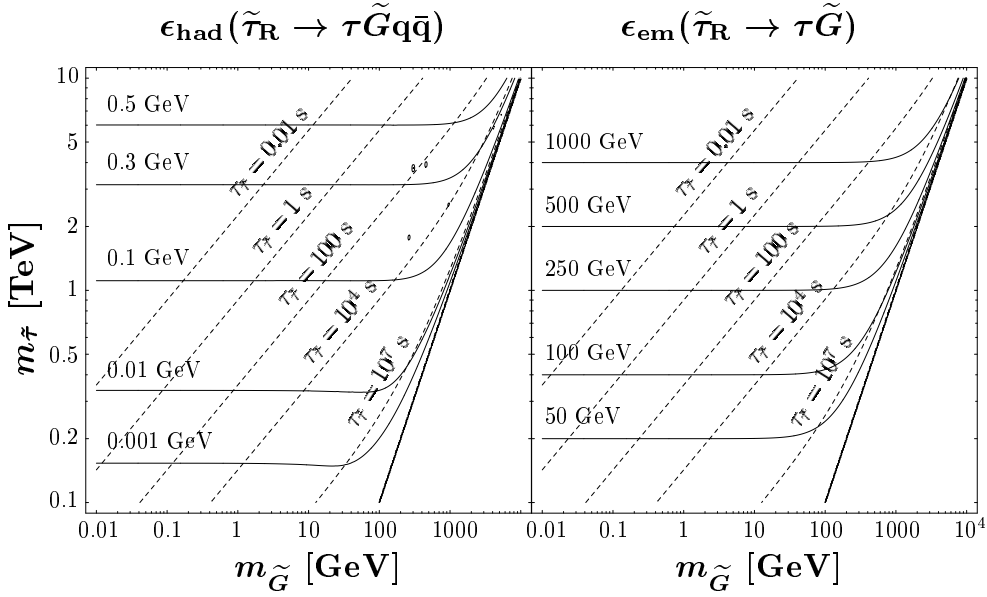


Figure 10: Contours of the hadronic energy ϵ_{had} (solid lines, left plot) and the electromagnetic energy $\epsilon_{\text{em}} = 0.5 E_{\tau}$ (solid lines, right plot) released in the decay of a single right-handed stau in the parameter space spanned by $m_{\tilde{G}}$ and $m_{\tilde{\tau}}$. The dashed contours indicate stau lifetimes of $\tau_{\tilde{\tau}} = 0.01, 1, 100, 10^4,$ and 10^7 s (from the upper left to the lower right).

interconversion processes triggered by mesons, which become relevant for $\tau_{\text{NLSP}} \lesssim 100$ s. For $10^7 \text{ s} \lesssim \tau_{\text{NLSP}} \lesssim 10^{12} \text{ s}$, the upper limits on purely electromagnetic energy release become as severe as the hadronic ones as can be seen from the lower part of Fig. 9. For more details on these limits and their interpretation, we refer to the original papers [29, 31].

In the following we will work with one severe and one conservative upper limit for both hadronic and electromagnetic energy release irrespective of the details. The severe limits are given by the solid (black) lines in conjunction with the dashed (red) lines. The conservative limits are obtained from combinations of the thin dash-dotted (yellow) and dotted (blue) curves.

4.2 Upper Limits on the Abundance of Charged Slepton NLSPs before their Decay

Let us focus again on scenarios with a charged slepton NLSP decaying late into the gravitino LSP. The corresponding (average) electromagnetic/hadronic energy emitted in a single charged slepton NLSP decay $\epsilon_{\text{em,had}}$ was studied in Secs. 2 and 3. From the nucleosynthesis bounds on $\xi_{\text{em,had}} (= \epsilon_{\text{em,had}} Y_{\text{NLSP}})$ discussed above, we now derive upper limits on the yield of charged slepton NLSPs before their decay. Once the yield is computed, the limits presented in this section can be transformed into bounds on the masses of the charged slepton NLSP and the gravitino LSP as will be demonstrated in Sec. 6. Since the extracted limits are sensitive to the nucleosynthesis bounds, we will show our results for both the severe and the conservative limits on $\xi_{\text{em,had}}$ defined above.

For a better understanding of the limits given below, Fig. 10 shows contours of the life-

Upper Limits on $Y_{\tilde{\tau}} = n_{\tilde{\tau}}/s$ prior to Stau NLSP Decays

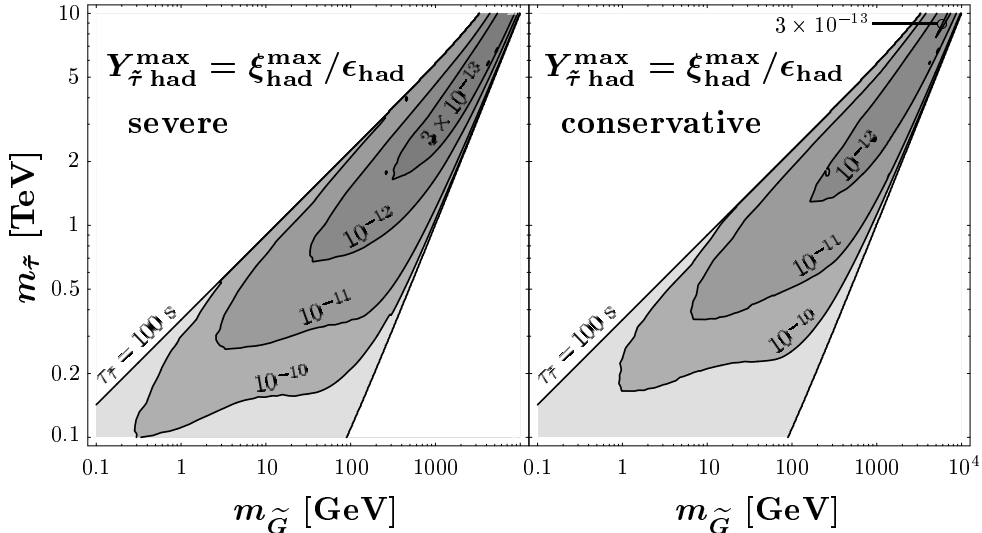


Figure 11: Upper limits on the yield of right-handed stau NLSPs before their decay, $Y_{\tilde{\tau}}^{\max} = \xi_{\text{had}}^{\max}/\epsilon_{\text{had}}$, as obtained from the severe (left) and the conservative (right) upper limits on late hadronic energy injection specified at the end of Sec. 4.1. The contour lines indicate $Y_{\tilde{\tau}}^{\max} = 3 \times 10^{-13}$, 10^{-12} , 10^{-11} , and 10^{-10} (from the upper right to the lower left). A darker shading implies a smaller value of $Y_{\tilde{\tau}}^{\max}$.

time of the right-handed stau NLSP (dashed lines) together with contours of the hadronic energy release ϵ_{had} (solid lines, left) obtained from (3.5) and the representative electromagnetic energy release $\epsilon_{\text{em}} = 0.5 E_{\tau}$ (solid lines, right) in the parameter space spanned by $m_{\tilde{G}}$ and $m_{\tilde{\tau}}$. At each point in the considered parameter space, one finds $\epsilon_{\text{had}} \ll \epsilon_{\text{em}}$ and might naively think that the constraints from hadronic energy injection are negligible. This is not the case since $\xi_{\text{had}}^{\max} \ll \xi_{\text{em}}^{\max}$ for $\tau_{\tilde{\tau}} \lesssim 10^7$ s. (For a given $\tau_{\tilde{\tau}} = \tau_{\text{NLSP}}$, the upper limits on ξ_{had} and ξ_{em} can be read directly from the curves shown in the upper and lower part of Fig. 9 respectively.)

Let us comment on the region in the $(m_{\tilde{G}}, m_{\tilde{\tau}})$ plane for which constraints will be provided. Studying gravitino LSP scenarios, we are interested only in the region $m_{\tilde{G}} < m_{\tilde{\tau}}$. Moreover, only stau masses $m_{\tilde{\tau}} \gtrsim 100$ GeV are considered since the searches for long-lived charged particles at LEP show that masses less than 97.5 GeV can be excluded at 95% CL for smuons and staus with a lifetime $\tau_{\tilde{1}} \geq 10^{-6}$ s [55]. (The corresponding mass bound for long-lived selectrons is 91 GeV.) As already mentioned, we concentrate on late decays, $\tau_{\tilde{\tau}} \gtrsim 100$ s, for which the hadronic constraints are most severe due to hadro-dissociation processes. No limits will be provided for stau lifetimes of $\tau_{\tilde{\tau}} < 100$ s, where the constraints on ξ_{had} are weaker anyhow as can be seen in the upper part of Fig. 9.

In Fig. 11 we give the upper limits on the yield of right-handed stau NLSPs before their decay, $Y_{\tilde{\tau}}^{\max} = \xi_{\text{had}}^{\max}/\epsilon_{\text{had}}$, as obtained from the severe (left) and the conservative (right) upper limit on late hadronic energy injection specified at the end of Sec. 4.1. With ϵ_{had} computed from (3.5), this is one of the main results of this paper. We show contours

for the values $Y_{\tilde{\tau}\text{had}}^{\text{max}} = 3 \times 10^{-13}$, 10^{-12} , 10^{-11} , and 10^{-10} (from the upper right to the lower left), where a darker shading implies a smaller value of $Y_{\tilde{\tau}\text{had}}^{\text{max}}$ and thus a more severe limit on $Y_{\tilde{\tau}}$. One finds that the upper limits $Y_{\text{had}}^{\text{max}}$ become serious for $m_{\tilde{G}} \gtrsim 100$ GeV and $m_{\tilde{\tau}} \gtrsim 0.7$ TeV.

Constraints from late electromagnetic energy injection, $Y_{\tilde{\tau}\text{em}}^{\text{max}} = \xi_{\text{em}}^{\text{max}}/\epsilon_{\text{em}}$, can become more severe than the ones from hadronic energy injection for $\tau_{\tilde{\tau}} \gtrsim 10^4$ s. We therefore combine the hadronic and electromagnetic constraints to determine the nucleosynthesis bounds on the yield of right-handed stau NLSPs before their decay:

$$Y_{\tilde{\tau}\text{BBN}}^{\text{max}} = \min(Y_{\tilde{\tau}\text{had}}^{\text{max}}, Y_{\tilde{\tau}\text{em}}^{\text{max}}) . \quad (4.9)$$

In Fig. 12 the resulting severe (left) and conservative (right) bounds—obtained with ϵ_{had} computed from (3.5) and $\epsilon_{\text{em}} = 0.3 E_{\tau}$ (top), $0.5 E_{\tau}$ (middle), and E_{τ} (bottom)—are shown, where the contour lines indicate the upper limits $Y_{\tilde{\tau}\text{BBN}}^{\text{max}} = 10^{-14}$, 10^{-13} , 10^{-12} , 10^{-11} , and 10^{-10} (as labeled) and a darker shading implies a more severe limit on $Y_{\tilde{\tau}}$. The sensitivity on ϵ_{em} is most pronounced for decays at $10^7 \text{ s} \lesssim t \lesssim 10^{12} \text{ s}$, which are the cosmic times at which the constraints from electromagnetic energy release become important. Recall that the (electromagnetic) constraints obtained for $\epsilon_{\text{em}}(\tilde{\tau} \rightarrow \tau \tilde{G}) = E_{\tau}$ are overly restrictive for stau NLSP scenarios as discussed in Sec. 2. Thus, a stau NLSP scenario which respects these constraints preserves the successful predictions of primordial nucleosynthesis.

Let us comment on the constraints in the alternative selectron NLSP and smuon NLSP scenarios. The bounds from hadronic energy injection shown in Fig. 11 can be applied directly to \tilde{e}_R or $\tilde{\mu}_R$ NLSP scenarios by performing the obvious substitutions $Y_{\tilde{\tau}} \rightarrow Y_{\tilde{e},\tilde{\mu}}$ and $m_{\tilde{\tau}} \rightarrow m_{\tilde{e},\tilde{\mu}}$. To take into account also the electromagnetic energy injection, we recall from Sec. 2 that the electromagnetic energy release from the decay of a single selectron or smuon NLSP is described respectively by $\epsilon_{\text{em}}(\tilde{e} \rightarrow e \tilde{G}) \simeq E_e$ and $\epsilon_{\text{em}}(\tilde{\mu} \rightarrow \mu \tilde{G}) \approx 0.3 E_{\mu}$ for $\tau_{\tilde{\mu}} \gtrsim 1.5 \times 10^4$ s. Thus, the upper limits on the abundance of selectron and smuon NLSPs before their decay—derived from both hadronic and electromagnetic nucleosynthesis constraints—can be read respectively from the plots at the bottom and the top in Fig. 12 once the obvious substitutions have been performed.

5. Gravitino Dark Matter from Charged Slepton NLSP Decays

In this section we consider the non-thermal production (NTP) of gravitino dark matter from late decays of charged slepton NLSPs. Additional upper limits on the yield of the charged slepton NLSPs before their decay can be obtained since the resulting gravitino density cannot exceed the observed dark matter density. We also provide estimates of the present free-streaming velocity and the comoving free-streaming scale of gravitino dark matter from charged slepton NLSP decays. Associated limits from observations of small-scale structure and early reionization are discussed.

5.1 Relic Gravitino Density from NLSP Decays

Since each NLSP decays into one gravitino LSP, the resulting relic density of gravitino dark matter is governed by the abundance of the NLSPs before their decay. Using $h =$

Upper Limits on $Y_{\tilde{\tau}} = n_{\tilde{\tau}}/s$ prior to Stau NLSP Decays

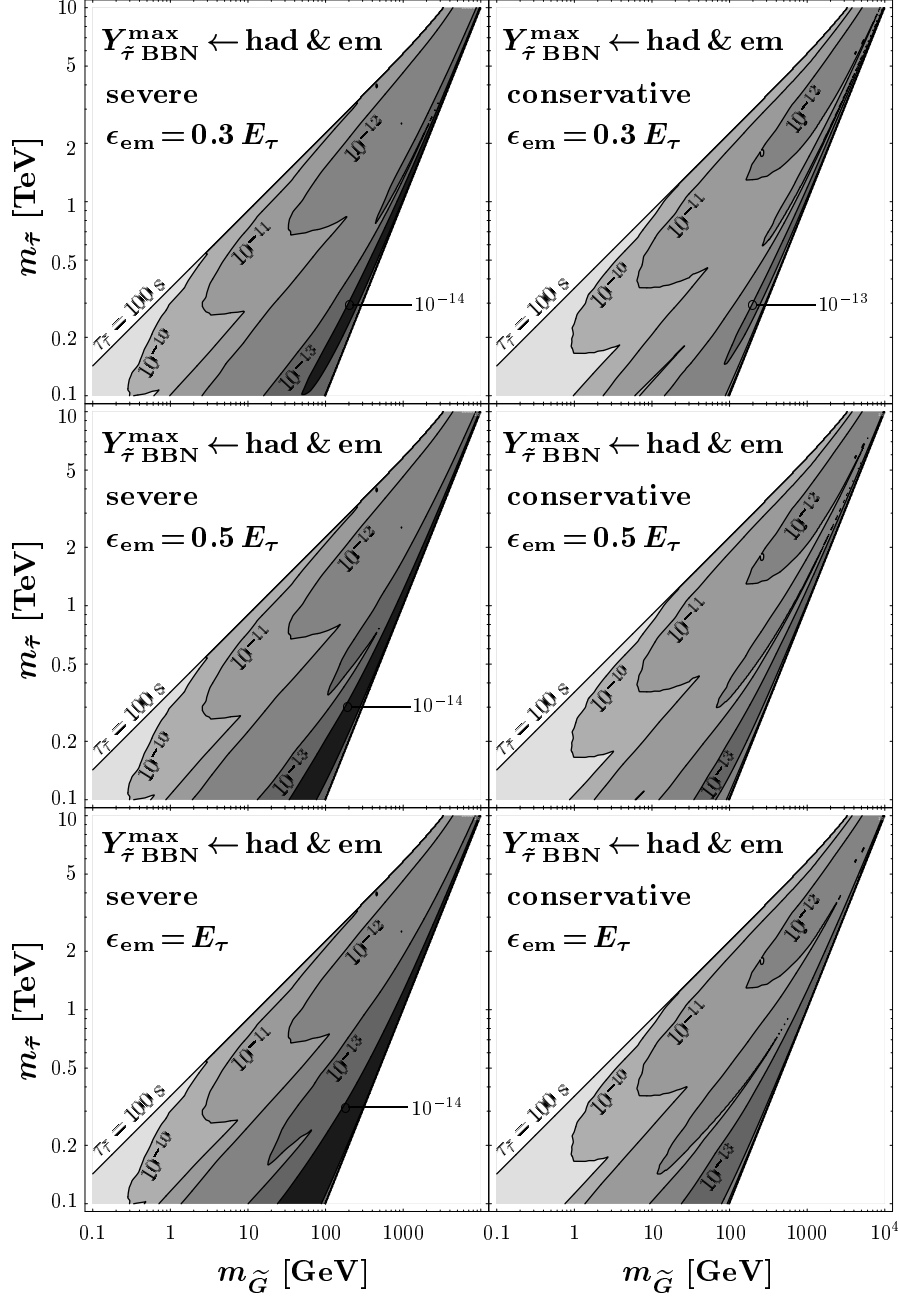


Figure 12: Upper limits on the yield of right-handed stau NLSPs before their decay, $Y_{\tilde{\tau}\text{BBN}}^{\text{max}} = \min(Y_{\tilde{\tau}\text{had}}^{\text{max}}, Y_{\tilde{\tau}\text{em}}^{\text{max}})$, as obtained from the severe (left) and the conservative (right) upper limits on late hadronic and electromagnetic energy injection specified at the end of Sec. 4.1. We computed $Y_{\tilde{\tau}\text{had}}^{\text{max}}$ from (3.5) and $Y_{\tilde{\tau}\text{em}}^{\text{max}}$ for $\epsilon_{\text{em}} = 0.3 E_{\tau}$ (top), $0.5 E_{\tau}$ (middle), and E_{τ} (bottom). Smaller values of $Y_{\tilde{\tau}\text{BBN}}^{\text{max}}$ are indicated by a darker shading.

$0.71_{-0.03}^{+0.04}$ [52, 7] to parametrize the Hubble constant $H_0 = 100 h \text{ km/sec/Mpc}$, the density

parameter of gravitinos produced non-thermally in late NLSP decays reads [13, 15]

$$\Omega_{\tilde{G}}^{\text{NTP}} h^2 = m_{\tilde{G}} Y_{\text{NLSP}} s(T_0) h^2 / \rho_c, \quad (5.1)$$

where $\rho_c/[s(T_0)h^2] = 3.6 \times 10^{-9} \text{ GeV}$ as obtained from the critical density $\rho_c/h^2 = 8.1 \times 10^{-47} \text{ GeV}^4$, the present temperature $T_0 = 2.73 \text{ K} \equiv 2.35 \times 10^{-13} \text{ GeV}$, and the number of effectively massless degrees of freedom governing the entropy density today $g_{*S}(T_0) = 3.91$. The observed density of cold dark matter (95% CL) [52, 7]¹

$$\Omega_{\text{CDM}}^{\text{obs}} h^2 = 0.113_{-0.018}^{+0.016} \quad (5.2)$$

thus gives the following upper limit on the yield of the NLSPs before their decay:

$$Y_{\text{NLSP CDM}}^{\text{max}} = f \frac{\Omega_{\text{CDM}}^{\text{max}} h^2}{m_{\tilde{G}}} \frac{\rho_c}{s(T_0) h^2} = 4.7 \times 10^{-12} f \left(\frac{\Omega_{\text{CDM}}^{\text{max}} h^2}{0.129} \right) \left(\frac{100 \text{ GeV}}{m_{\tilde{G}}} \right) \quad (5.3)$$

where f denotes the fraction of dark matter which is assumed to be provided by NLSP decays, $\Omega_{\tilde{G}}^{\text{NTP}} = f \Omega_{\text{CDM}}^{\text{obs}}$. We also consider values of f less than one since thermal production of gravitinos in the early Universe can contribute significantly to $\Omega_{\text{CDM}}^{\text{obs}}$; cf. Sec. 7. Note that (5.1) and (5.3) apply not only to charged slepton NLSPs but also to any NLSP decaying into the gravitino LSP in SUSY scenarios with conserved R-parity.

In Fig. 13 we show $Y_{\text{NLSP CDM}}^{\text{max}}$ for scenarios with $f = 1$ (grey band) and $f = 0.01$ and 0.1 (solid lines, as labeled). For charged slepton NLSP cases, a comparison with the BBN bounds—given in Fig. 12—shows that the bounds from $\Omega_{\text{CDM}}^{\text{obs}}$ become more severe towards larger values of $m_{\tilde{G}}$, particularly for small values of f .

5.2 Free Streaming of Gravitinos and Constraints from Small-Scale Structure

The extremely weakly interacting gravitinos can be treated as collisionless dark matter. With a non-negligible velocity, they can stream out of overdense regions and into underdense regions before the time of matter–radiation equality. This free streaming leads to an erasure of structure on scales below the comoving free-streaming scale λ_{FS} [57]. Thus, observations and simulations of cosmic structures can provide severe upper limits on λ_{FS} or, equivalently, on the present free-streaming velocity v_{FS}^0 of gravitino dark matter [13, 27]. On the other hand, numerical simulations of cold (i.e. $v_{\text{FS}}^0 \simeq 0$) dark matter predict too much power on small scales ($\lesssim 1 \text{ Mpc}$), such as an excess in the number of low mass halos and over dense halo cores. These problems could be resolved in warm dark matter scenarios (see [69, 62, 63] and references therein) including those in which gravitinos with a non-negligible velocity dispersion v_{FS}^0 dominate $\Omega_{\text{CDM}}^{\text{obs}}$ [58, 59].

For gravitino dark matter produced non-thermally in late NLSP decays, the comoving free-streaming scale at the time of matter–radiation equality t_{eq} can be estimated as follows

$$\lambda_{\text{FS}}^{\tilde{G}^{\text{NTP}}} = \int_{\tau_{\text{NLSP}}}^{t_{\text{eq}}} dt \frac{v(t)}{a(t)} = v_0 t_{\text{eq}} (1 + z_{\text{eq}})^2 \ln \left(\sqrt{\frac{t_{\text{eq}}}{\tau_{\text{NLSP}}} \frac{1 + \sqrt{1 + v_0^2 (1 + z_{\text{eq}})^2}}{1 + \sqrt{1 + v_0^2 (1 + z_{\text{eq}})^2 (t_{\text{eq}}/\tau_{\text{NLSP}})}}} \right), \quad (5.4)$$

¹The value given in (5.2) can be updated taking into account the recent three year results of the Wilkinson Microwave Anisotropy Probe (WMAP) [56]. However, this would affect our results at most marginally.

$Y_{\text{NLSP}}^{\text{max}} = n_{\text{NLSP}}^{\text{max}}/s$ prior to NLSP Decays

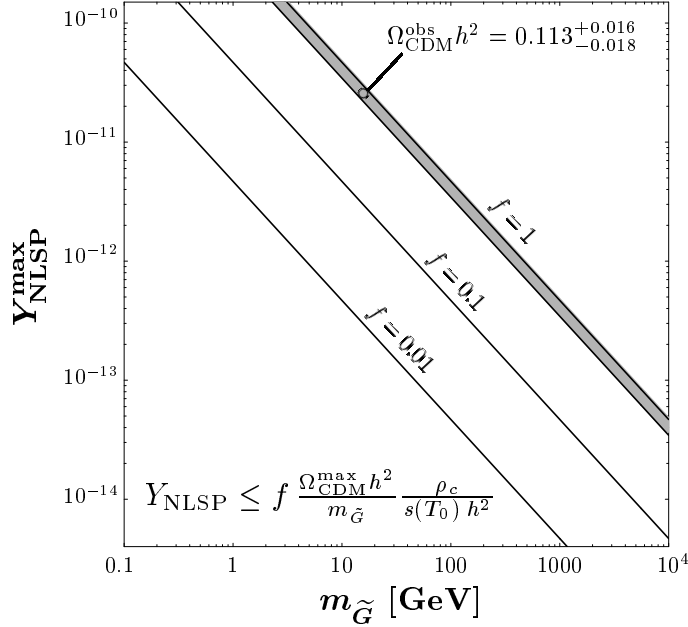


Figure 13: Upper limits on the yield of the NLSPs before their decay, $Y_{\text{NLSP CDM}}^{\text{max}}$, from the observed density of dark matter $\Omega_{\text{CDM}}^{\text{obs}} h^2$ as a function of the gravitino mass $m_{\tilde{G}}$. The grey band indicates the values of $(m_{\tilde{G}}, Y_{\text{NLSP}}^{\text{max}})$ for which $\Omega_{\tilde{G}}^{\text{NTP}} h^2$ agrees with $\Omega_{\text{CDM}}^{\text{obs}} h^2 = 0.113^{+0.016}_{-0.018}$ (95% CL) [52, 7]. The region above the grey band is excluded. The solid lines show the limits obtained for $f \Omega_{\text{CDM}}^{\text{max}} h^2$ with $\Omega_{\text{CDM}}^{\text{max}} h^2 = 0.129$ and $f = 0.01$ and 0.1 (as labeled).

with the cosmic scale factor $a(t)$, the gravitino velocity $v(t) = |\vec{p}(t)|/\sqrt{|\vec{p}(t)|^2 + m_{\tilde{G}}^2}$ and its present value $v_0 \equiv v_{\text{FS}}^0$, which is assumed to be non-relativistic. The time and redshift at matter–radiation equality are given respectively by

$$z_{\text{eq}} = 3224 \left(\frac{\Omega_{\text{m}} h^2}{0.135} \right) \quad \text{and} \quad t_{\text{eq}} = 4.7 t_0 \times 10^{-6} = 2.0 \times 10^{12} \text{ s} , \quad (5.5)$$

where $t_0 = 4.3 \times 10^{17} \text{ s}$ is the age of the Universe in a cosmological model with matter density $\Omega_{\text{m}} = 0.27$, radiation density $\Omega_{\text{R}} = 5 \times 10^{-5}$, and cosmological constant $\Omega_{\Lambda} = 0.73$. In the estimate (5.4), we use again the sudden decay approximation by assuming that the gravitinos are injected when the cosmic time t equals the NLSP lifetime τ_{NLSP} . For $\tau_{\text{NLSP}} \ll t_{\text{eq}}$, the estimate (5.4) agrees with the one given in Refs. [60, 61],

$$\lambda_{\text{FS}}^{\tilde{G}\text{NTP}} \Big|_{\tau_{\text{NLSP}} \ll t_{\text{eq}}} \simeq \int_0^{t_{\text{eq}}} dt \frac{v(t)}{a(t)} = v_0 t_{\text{eq}} (1+z_{\text{eq}})^2 \ln \left(\sqrt{1 + \frac{1}{v_0^2 (1+z_{\text{eq}})^2}} + \frac{1}{v_0 (1+z_{\text{eq}})} \right) . \quad (5.6)$$

In charged slepton NLSP scenarios, the non-thermally produced gravitinos originate mainly from the 2-body decay $\tilde{\text{L}}_{\text{R}} \rightarrow \text{l}\tilde{\text{G}}$ discussed in Sec. 2. The contribution of the 4-body decay $\tilde{\text{L}}_{\text{R}} \rightarrow \text{l}\tilde{\text{G}}\text{q}\bar{\text{q}}$ to $\Omega_{\tilde{G}}^{\text{NTP}}$ is less than 1% in the considered parameter range as can be seen in Figs. 4 and 5. Accordingly, the initial momentum of the gravitino from the 2-body

decay $\tilde{\tau}_R \rightarrow \tau \tilde{G}$

$$|\vec{p}_{\tilde{G}}(t_i)| = \frac{m_{\tilde{\tau}}^2 - m_{\tilde{G}}^2 - m_{\tau}^2}{2m_{\tilde{\tau}}}, \quad (5.7)$$

governs the gravitino spectrum, which is monochromatic in the sudden decay ($t_i = \tau_{\tilde{\tau}}$) approximation. (A treatment of the phase space distribution beyond the sudden decay approximation can be found in Ref. [58].) Under the reasonable assumption that the gravitino momentum is non-relativistic today, $|\vec{p}_{\tilde{G}}(t_0)| = m_{\tilde{G}} v_0$, one can derive directly the free-streaming velocity of gravitinos today [27]. With the lifetime $\tau_{\tilde{\tau}}$ given by the inverse of the decay width (2.2), we obtain the following result for the present free-streaming velocity of gravitinos from stau NLSP decays in the limit $m_{\tau} \rightarrow 0$

$$v_{\text{FS}}^0 \tilde{G}^{\text{NTP}} = 0.024 \frac{\text{km}}{\text{s}} \left(\frac{g_*(t_i = \tau_{\tilde{\tau}})}{3.36} \right)^{1/4} \left(\frac{m_{\tilde{\tau}}}{1 \text{ TeV}} \right)^{-3/2} \left(1 - \frac{m_{\tilde{G}}^2}{m_{\tilde{\tau}}^2} \right)^{-1}, \quad (5.8)$$

where $g_*(t)$ is the effective number of relativistic degrees of freedom governing the energy density. The result (5.8) is valid for gravitinos from stau NLSP decays in the radiation-dominated epoch, $\tau_{\tilde{\tau}} < t_{\text{eq}}$.

For warm dark matter with a thermal spectrum—such as light ($m_{\tilde{G}} \lesssim 100 \text{ eV}$) gravitinos once in thermal equilibrium [8]—constraints on the associated free-streaming length $\lambda_{\text{FS}}^{\text{WDM}}$ and the present free-streaming velocity $v_{\text{FS}}^0 \text{WDM}$ have been derived from observations and simulations of cosmic structures. As demonstrated in [60], these limits can be adopted to some extent to non-thermally produced dark matter with a monochromatic spectrum. Thus, we summarize the limits obtained for warm dark matter with a thermal spectrum and then discuss the implications for gravitino dark matter from charged slepton NLSP decays. A similar study with emphasis on constraints from early reionization can be found in [27].

In warm dark matter investigations of cosmic structure formation, it is typically assumed that all dark matter consists of a particle species with mass m_{WDM} that was once in thermal equilibrium with the primordial plasma and freezes out with a thermal spectrum while relativistic at $T_{\text{f}} \gg m_{\text{WDM}}$. For a Majorana fermion of spin 1/2, i.e., a fermion with two internal degrees of freedom, the resulting relic density reads

$$\Omega_{\text{WDM}} h^2 = 0.115 \left(\frac{100}{g_{*S}(T_{\text{f}})} \right) \left(\frac{m_{\text{WDM}}}{100 \text{ eV}} \right) \quad (5.9)$$

so that the requirement $\Omega_{\text{CDM}}^{\text{obs}} = \Omega_{\text{WDM}}$ fixes $g_{*S}(T_{\text{f}})$ for a given m_{WDM} . This, in turn, determines the root mean squared value of the warm dark matter velocity dispersion today

$$(v_{\text{FS}}^{\text{rms},0})_{\text{WDM}} = 0.77 \frac{\text{km}}{\text{s}} \left(\frac{\Omega_{\text{WDM}} h^2}{0.113} \right)^{1/3} \left(\frac{100 \text{ eV}}{m_{\text{WDM}}} \right)^{4/3}. \quad (5.10)$$

The obtained upper limits on $(v_{\text{FS}}^{\text{rms},0})_{\text{WDM}}$ are thus often expressed as lower limits on m_{WDM} . Note that the constraint $\Omega_{\text{CDM}}^{\text{obs}} = \Omega_{\text{WDM}}$ implies $g_{*S}(T_{\text{f}}) \gtrsim 500$ for $m_{\text{WDM}} \gtrsim 0.5 \text{ keV}$, which is more than about five (two) times the number of degrees of freedom in the standard model (MSSM) and requires physics beyond the MSSM (see also the discussion

Table 1: Constraints on warm dark matter models from observations and simulations of cosmic structures. The lower limits on the mass, $m_{\text{WDM}}^{\text{min}}$, are taken from the corresponding references. The values for $(v_{\text{FS}}^{\text{rms},0})_{\text{WDM}}^{\text{max}}$ and $(\lambda_{\text{FS}})_{\text{WDM}}^{\text{max}}$ are derived from $m_{\text{WDM}}^{\text{min}}$ using (5.10) and (5.6), respectively.

Probe/Observable	$m_{\text{WDM}}^{\text{min}}$ [keV]	$(v_{\text{FS}}^{\text{rms},0})_{\text{WDM}}^{\text{max}}$ [km/s]	$(\lambda_{\text{FS}})_{\text{WDM}}^{\text{max}}$ [Mpc]	Ref.
Dwarf spheroidal galaxies	0.7	0.06	0.64	[63]
Lyman- α forest at $z \simeq 3$	0.75	0.05	0.59	[64]
Lyman- α forest at $z \simeq (2 - 3)$	0.55	0.08	0.84	[65]
Supermassive black hole at $z \simeq 5.8$	0.5	0.09	0.94	[66]
Cosmological reionization by $z \simeq 5.8$	0.75	0.05	0.59	[66]

in [62]). Since $t_f \ll t_{\text{eq}}$, we can use expression (5.6) with $v_0 = (v_{\text{FS}}^{\text{rms},0})_{\text{WDM}}$ to estimate the comoving free-streaming scale of the thermal relic at matter–radiation equality, $\lambda_{\text{FS}}^{\text{WDM}}$.

In Table 1 we list constraints on m_{WDM} obtained in warm dark matter studies of cosmic structure formation. The considered probes include the maximum observed phase-space density in dwarf spheroidal galaxies [63], the observed properties of the Lyman- α forest in quasar spectra [64, 65], the supermassive black hole believed to power the quasar SDSS 1044-1215, and the reionization inferred from ionized hydrogen in the intergalactic medium [66]. With the lower bound on the mass, $m_{\text{WDM}}^{\text{min}}$, taken from the given reference, the values for $(v_{\text{FS}}^{\text{rms},0})_{\text{WDM}}^{\text{max}}$ and $(\lambda_{\text{FS}})_{\text{WDM}}^{\text{max}}$ were derived from (5.10) and (5.6), respectively. The limits from the various probes are basically consistent. One finds that present free-streaming velocities of $(v_{\text{FS}}^{\text{rms},0})_{\text{WDM}} \gtrsim (0.05 - 0.09)$ km/s are disfavored if all dark matter consists of warm dark matter with such a velocity dispersion. From cosmological reionization by redshift $z = 5.8$, a somewhat more severe limit of $m_{\text{WDM}} \gtrsim 1.2$ keV has also been discussed in [66], which corresponds to $(v_{\text{FS}}^{\text{rms},0})_{\text{WDM}} \lesssim 0.03$ km/s. With evidence for cosmological reionization at higher redshift, the limit on $(v_{\text{FS}}^{\text{rms},0})_{\text{WDM}}$ can become even more severe since warm dark matter with a sizeable velocity dispersion delays the formation of an early generation of stars or quasars, which provides the most natural explanation for early reionization. Indeed, the polarization analysis of the three year WMAP data constrains the optical depth to $\tau = 0.088_{-0.034}^{+0.028}$, which points to reionization at $z = 10.9_{-2.3}^{+2.7}$ in a model with instantaneous reionization [67]. These new results replace the ones from the analysis of the first year WMAP data, in which $\tau = 0.17 \pm 0.06$ was interpreted to originate from reionization at $z \sim 20$ [52]. In the light of the polarization analysis of the three year WMAP observations [67], we do not list the (possibly overly restrictive) limit $m_{\text{WDM}} \gtrsim 10$ keV, corresponding to $(v_{\text{FS}}^{\text{rms},0})_{\text{WDM}} \lesssim 0.002$ km/s, which was derived from the first year WMAP observations [68] and discussed in [27] for gravitinos from NLSP decays.

In Fig. 14 we show the contours of the present free-streaming velocity of gravitinos from stau NLSP decays obtained from (5.8) with $g_*(t \gtrsim 10 \text{ s}) = 3.36$. The values $v_{\text{FS}}^0 \tilde{G}^{\text{NTP}} = 0.002, 0.004, 0.01, 0.04, 0.09, 0.3, \text{ and } 0.8$ km/s (from top to bottom) correspond to the present values of the velocity dispersion of warm dark matter with $m_{\text{WDM}} = 10, 5, 2, 1, 0.5, 0.2, \text{ and } 0.1$ keV, respectively. The contours can also be associated with the following values of the comoving free-streaming scale at matter–radiation equality: $\lambda_{\text{FS}}^{\tilde{G}^{\text{NTP}}} = 0.03,$

Present Velocity of Gravitinos from $\tilde{\tau} \rightarrow \tau \tilde{G}$

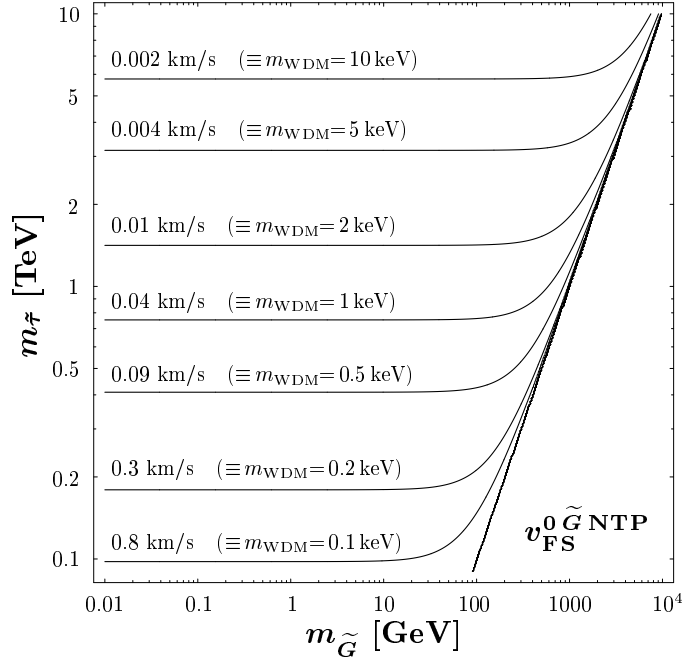


Figure 14: Contours of the present free-streaming velocities of gravitinos from stau NLSP decays, $v_{\text{FS}}^{0 \tilde{G} \text{NTP}}$, in the parameter space spanned by $m_{\tilde{G}}$ and $m_{\tilde{\tau}}$. The indicated values $v_{\text{FS}}^{0 \tilde{G} \text{NTP}} = 0.002, 0.004, 0.01, 0.04, 0.09, 0.3, \text{ and } 0.8$ km/s (from top to bottom) can be associated with the present velocity dispersion of warm dark matter made of thermal relics of mass $m_{\text{WDM}} = 10, 5, 2, 1, 0.5, 0.2, \text{ and } 0.1$ keV, respectively.

0.06, 0.2, 0.4, 1.0, 2.7, and 5.8 Mpc (from top to bottom).

In scenarios in which basically all dark matter consists of gravitinos from NLSP decays ($f \approx 1$)—also known as superWIMP gravitino dark matter scenarios [17, 18, 21]—the warm dark matter limits from Table 1 can be applied [60]. Accordingly, Fig. 14 shows that such scenarios with $m_{\tilde{\tau}} \lesssim 0.5$ TeV are in conflict with the constraints inferred from warm dark matter investigations of cosmological structure formation. This is a conservative limit. With a better understanding of cosmological reionization and the Next Generation Space Telescope [66], one could find that even values of the stau NLSP mass up to about 1 TeV are excluded. (The additional BBN constraints for superWIMP gravitino dark matter scenarios will be updated in Sec. 6.) However, if regions with $0.01 \text{ km/s} \lesssim v_{\text{FS}}^{0 \tilde{G} \text{NTP}} \lesssim 0.05 \text{ km/s}$ remain allowed, superWIMP gravitino dark matter could behave like warm dark matter made of thermal relics with $750 \text{ keV} \lesssim m_{\text{WDM}} \lesssim 2 \text{ keV}$ and thus resolve the small-scale structure problems of cold dark matter [13, 58, 59].

For superWIMP gravitino dark matter from charged NLSP decays at late times, $\tau_{\text{NLSP}} \gtrsim 10^7$ s, one might think that there is an additional suppression of power on sub-galactic scales due to the coupling of the charged NLSP to the photon–baryon fluid [70]. However, we will show explicitly that the BBN constraints exclude lifetimes of $\tau_{\text{NLSP}} \gtrsim 10^7$ s completely for the considered charged slepton NLSP scenarios with $f \approx 1$.

For scenarios in which only a fraction $f < 1$ of $\Omega_{\text{CDM}}^{\text{obs}}$ comprises of gravitinos from NLSP decays, the warm dark matter limits listed in Table 1 will be overly restrictive. In the limiting case in which the gravitinos behave as hot dark matter, existing constraints from studies of hot dark matter such as active neutrinos could be adopted [27]. However, these constraints apply only to the high velocity region below the contour $v_{\text{FS}}^0 \tilde{G}^{\text{NTP}} = 0.8$ km/s in Fig. 14, which is excluded anyhow either by the mass bounds from searches for long-lived charged particles at LEP [55] or—as will be shown below—by the BBN constraints. In the parameter region with $v_{\text{FS}}^0 \tilde{G}^{\text{NTP}} \lesssim 0.8$ km/s, dedicated N-body simulations are needed to extract reliable constraints for such mixed dark matter scenarios from cosmic structures on small scales. We postpone this non-trivial task for future work.

6. Bounds on the Gravitino and Charged Slepton NLSP Masses

In this section we use estimates of the abundance of charged slepton NLSPs before their decay to extract mass bounds for the gravitino LSP and the charged slepton NLSP from the cosmological constraints discussed above. Based on our exact treatment of the hadronic energy release, we present an update of the mass bounds given in Refs. [15, 21, 22]. We consider estimates of the charged slepton NLSP abundance prior to decay, which assume that the NLSPs were once in thermal equilibrium and decoupled before decaying into the gravitino LSP. In addition, we provide mass bounds for scenarios in which a fixed fraction f of the dark matter density consists of gravitinos from late decays of charged slepton NLSPs.

6.1 Estimates of the Abundance of Charged Slepton NLSPs before their Decay

The charged slepton NLSPs were in thermal equilibrium with the primordial plasma until the temperature of the Universe dropped below their freeze-out temperature of $T_f \simeq m_{\tilde{\tau}_1}/29 - m_{\tilde{\tau}_1}/25$ [15]. Since $T_f \ll m_{\tilde{\tau}_1}$, these NLSPs are already highly non-relativistic when they decouple from the thermal plasma and thus behave as cold thermal relics before their decay. This also demonstrates that the charged slepton NLSPs can indeed be considered to be at rest when decays into the gravitino LSP at temperatures $T \ll T_f$ are studied.

Although we do not have unambiguous evidence for temperatures of the Universe higher than $T \approx 1$ MeV (i.e. the temperature at primordial nucleosynthesis), we assume a cosmological scenario with temperatures above T_f at early times. This means temperatures higher than about at least 3 GeV which is the lowest possible value of T_f obtained from the smallest allowed mass of a long-lived charged slepton, $m_{\tilde{\tau}_1} \approx 100$ GeV [55]. Under this assumption, the NLSP abundance becomes independent of the reheating temperature after inflation.

Once the charged slepton NLSPs are decoupled from the thermal plasma, their yield $Y_{\tilde{\tau}_1} = n_{\tilde{\tau}_1}/s$ prior to their decay is given approximately by the value at freeze out: $Y_{\tilde{\tau}_1}(T) \approx Y_{\tilde{\tau}_1}^{\text{equil}}(T_f)$ for $T \lesssim T_f$; cf. [57, 71, 15] and references therein. The precise value of $Y_{\tilde{\tau}_1}(t = \tau_{\tilde{\tau}_1})$ depends on details of the NLSP decoupling, which are governed by the mass spectrum and the couplings of the superparticles. Indeed, dedicated computer programs such as DarkSUSY [72] or micrOMEGAs [73] are available for the computation of the freeze out

and the resulting relic abundances of neutralinos and other weakly interacting massive particles (WIMPs) in a given SUSY model.

In this paper we consider the following estimates of the stau NLSP abundance

$$Y_{\tilde{\tau}}^{m_{\tilde{\tau}_1} \ll m_{\tilde{e}_1, \tilde{\mu}_1}} = 0.725 \times 10^{-12} \left(\frac{m_{\tilde{\tau}}}{1 \text{ TeV}} \right), \quad (6.1)$$

$$Y_{\tilde{\tau}}^{m_{\tilde{\tau}_1} \approx m_{\tilde{e}_1, \tilde{\mu}_1}} = 1.45 \times 10^{-12} \left(\frac{m_{\tilde{\tau}}}{1 \text{ TeV}} \right), \quad (6.2)$$

which are applicable for $m_{\tilde{\tau}} \gtrsim 100 \text{ GeV}$ as can be seen from the curves in Fig. 1 of Ref. [15]. These curves have been derived for $m_{\tilde{B}} = 1.1 m_{\tilde{\tau}}$ and purely right-handed lighter sleptons $\tilde{l}_1 = \tilde{l}_R$ (i.e. negligible left–right mixing of sleptons). Coannihilation processes of sleptons with binos have not been taken into account.

The estimate (6.1) is valid for a superparticle spectrum in which the stau NLSP mass is significantly below the masses of the lighter selectron and the lighter smuon. Because of $m_{\tilde{\tau}_1} \ll m_{\tilde{e}_1, \tilde{\mu}_1}$, the abundances of the lighter selectron and the lighter smuon are negligible at the time of the stau NLSP freeze out so that selectron/smuon–stau coannihilation processes can be ignored. Accordingly, the selectrons/smuons do not affect the freeze out of the stau NLSPs and the stau NLSP abundance is given by $Y_{\tilde{\tau}} \simeq n_{\tilde{\tau}}/s$ with $n_{\tilde{\tau}} \equiv n_{\tilde{\tau}_1} + n_{\tilde{\tau}_1^*}$.

The estimate (6.2) is valid for a superparticle spectrum in which the stau NLSP mass and the masses of the lighter selectron and smuon are nearly degenerate. Because of $m_{\tilde{\tau}_1} \approx m_{\tilde{e}_1, \tilde{\mu}_1}$, the abundances of the lighter selectron and the lighter smuon are comparable to the stau NLSP abundance and selectron/smuon–stau coannihilation processes are important [71, 15]. Although these coannihilation processes reduce the abundance of each lighter charged slepton species, the net abundance of the stau NLSP is doubled since $Y_{\tilde{\tau}}(\tau_{\tilde{\tau}}) \simeq Y_1(T_f) = (n_{\tilde{e}_1} + n_{\tilde{e}_1^*} + n_{\tilde{\mu}_1} + n_{\tilde{\mu}_1^*} + n_{\tilde{\tau}_1} + n_{\tilde{\tau}_1^*})/s$ as each lighter selectron/smuon decays eventually into one stau NLSP via $\tilde{e}_1(\tilde{\mu}_1) \rightarrow \tilde{\tau}_1 \tau \mu(e)$. Note however that these decays will be forbidden kinematically if the mass difference $m_{\tilde{e}_1, \tilde{\mu}_1} - m_{\tilde{\tau}_1}$ is smaller than the mass of the tau lepton. The lighter selectrons/smuons then decay directly into gravitinos and standard model particles. Thus, cosmological constraints have to be considered for each lighter charged slepton species separately. This affects the electromagnetic BBN constraints as can be seen from our discussion of the selectron/smuon NLSP scenarios in Sec. 2. The resulting mass bounds however will remain between the limiting curves shown below. In contrast to the electromagnetic BBN constraints, the hadronic ones from late ($\tau_{\tilde{l}} \gtrsim 100 \text{ s}$) decays of charged sleptons are equally valid for each charged slepton species ($\tilde{l}_1 = \tilde{l}_R$) as already mentioned in Sec. 3. The resulting mass bounds will therefore not be affected by the discussed precise slepton mass degeneracies.

In Fig. 15 we plot $Y_{\tilde{\tau}}$ as a function of $m_{\tilde{\tau}}$. The solid and dashed curves show the estimates (6.1) and (6.2) respectively. Note that the estimate (6.1) has also been used in Refs. [22, 74]. It is in good agreement with the result from micrOMEGAs obtained for $\tan \beta = 30$ in Ref. [19]. Also the other estimate (6.2) seems reasonable. For example, an only slightly higher stau NLSP abundance was found in Ref. [71] with slepton coannihilations taken into account.

We consider the estimates (6.1) and (6.2) as representative abundances. The actual stau NLSP abundance may be smaller or larger depending on the SUSY model realized

Estimates of $Y_{\tilde{\tau}}$ prior to $\tilde{\tau}$ NLSP Decays

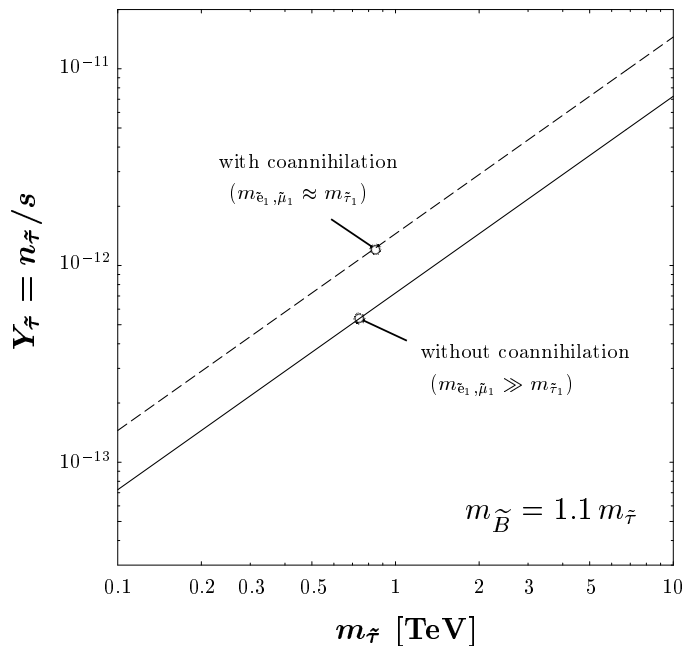


Figure 15: The yield of the stau NLSP prior to its decay, $Y_{\tilde{\tau}} \equiv n_{\tilde{\tau}}/s$ with $n_{\tilde{\tau}} \equiv n_{\tilde{\tau}_1} + n_{\tilde{\tau}_1^*}$, as a function of $m_{\tilde{\tau}}$. The solid and dashed curves show respectively the estimate for $m_{\tilde{\tau}_1} \ll m_{\tilde{e}_1, \tilde{\mu}_1}$ given in (6.1) and the one for $m_{\tilde{\tau}_1} \approx m_{\tilde{e}_1, \tilde{\mu}_1}$ given in (6.2). Both estimates are taken from Fig. 1 of Ref. [15] and have been derived for $m_{\tilde{B}} = 1.1 m_{\tilde{\tau}}$ and purely right-handed lighter sleptons, $\tilde{l}_1 = \tilde{l}_R$.

in nature. For example, for $m_{\tilde{\tau}} \lesssim m_{\tilde{B}} < 1.1 m_{\tilde{\tau}}$, the stau–bino coannihilation processes become important, thereby leading to an enhancement of the stau NLSP abundance [71]. On the other hand, a sizeable left–right mixing of the stau NLSP is associated with an increase of its MSSM couplings and thus with a reduction of the stau NLSP abundance [57]. Once the SUSY model realized in nature is probed at future colliders, we will be able to reduce such uncertainties in the computation of the stau NLSP yield. For a mainly right-handed stau NLSP, the resulting yield can then be confronted directly with the cosmological upper limits given in Figs. 11–13 above.

6.2 Mass Bounds from the Estimates of the Charged Slepton NLSP Abundance

Let us now confront the stau NLSP abundance (6.1) obtained for $m_{\tilde{\tau}_1} \ll m_{\tilde{e}_1, \tilde{\mu}_1}$ with the BBN constraints shown in Fig. 12 and the $\Omega_{\text{CDM}}^{\text{obs}}$ constraints shown in Fig. 13. This leads to the bounds on $m_{\tilde{G}}$ and $m_{\tilde{\tau}}$ shown in Fig. 16. The observed dark matter density $\Omega_{\text{CDM}}^{\text{obs}} h^2$ excludes the region above the grey band. The grey band marks the region of superWIMP gravitino dark matter scenarios [17, 18, 21] in which $\Omega_{\text{CDM}}^{\text{obs}}$ is provided by gravitinos from stau NLSP decays alone, $\Omega_G^{\text{NTP}} \approx \Omega_{\text{CDM}}^{\text{obs}}$. Only 10% (1%) of $\Omega_{\text{CDM}}^{\text{obs}}$ is provided by gravitinos from stau NLSP decays for scenarios that fall onto the thin solid line labeled by $f = 0.1$ ($f = 0.01$). The thick solid (red) and thick dashed (blue) curves show the limits from late hadronic and electromagnetic energy injection, respectively, for both the severe (left plot) and the conservative (right plot) BBN bounds. The region to the left of the corresponding

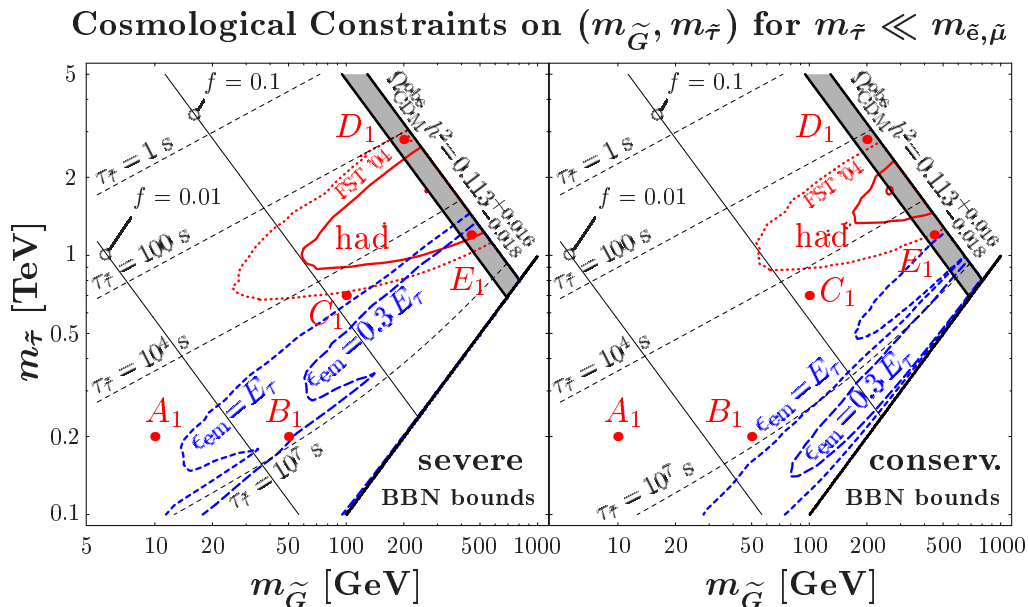


Figure 16: Exclusion limits for $m_{\tilde{G}}$ and $m_{\tilde{\tau}}$ from the severe (left plot) and conservative (right plot) BBN bounds on electromagnetic (thick dashed lines, blue) and hadronic (thick solid lines, red) energy release and from $\Omega_{\text{CDM}}^{\text{obs}}$ (grey band) obtained with the stau NLSP abundance (6.1). Allowed is the region from the grey band downwards, to the left of the thick dashed curve(s), and outside of the area enclosed by the thick solid curve. On the grey band and on the thin solid lines labeled by $f = 0.1$ and $f = 0.01$, gravitinos from stau NLSP decays provide 100%, 10%, and 1% of $\Omega_{\text{CDM}}^{\text{obs}}$, respectively. The thin dashed lines show contours of $\tau_{\tilde{\tau}} = 1$ s, 100 s, 10^4 s, and 10^7 s (from top to bottom). Our study concentrates on $\tau_{\tilde{\tau}} \gtrsim 100$ s. The dotted (red) line labeled with “FST ’04” shows the outdated hadronic BBN constraint from the ϵ_{had} estimate of Ref. [21]. The thick (red) dots indicate the benchmark scenarios A_1 – E_1 that will be introduced in Sec. 9 (cf. Table 2).

curves remains allowed. For the electromagnetic BBN constraints, we obtain the short-dashed and the long-dashed curves with the limiting values $\epsilon_{\text{em}} = E_{\tilde{\tau}}$ and $\epsilon_{\text{em}} = 0.3 E_{\tilde{\tau}}$ respectively. The actual BBN exclusion limit from late electromagnetic energy injection will fall between these two curves. The dotted (red) line shows the outdated hadronic BBN constraint obtained with the simplified estimate (3.6) from Ref. [21]. The thick (red) dots indicate the benchmark scenarios A_1 – E_1 that will be introduced and discussed in Sec. 9. The thin dashed lines show contours of the stau NLSP lifetime of $\tau_{\tilde{\tau}} = 1$ s, 100 s, 10^4 s, and 10^7 s (from top to bottom). Recall that we focus our investigation on late decays $\tau_{\tilde{\tau}} \gtrsim 100$ s. For shorter lifetimes $\tau_{\tilde{\tau}}$, additional exclusion limits may arise from decays of the tau lepton into mesons since these mesons can trigger proton–neutron interconversion processes [29].

From a comparison of our new result for the hadronic BBN constraint labeled “had” with the outdated one labeled “FST ’04”, we find that the previous estimate (3.6) from Ref. [21] leads to overly restrictive limits. Accordingly, the hadronic BBN constraints given in Refs. [22, 23], which were obtained with the estimate of [21], are overly restrictive.

Our results on hadronic energy release have consequences for the possible existence of superWIMP gravitino dark matter scenarios ($f \approx 1$) with charged slepton NLSPs. Because

of the previously overestimated hadronic energy release, such scenarios were expected to be completely excluded for $\tau_{\tilde{\tau}} \gtrsim 100$ s by the severe BBN bounds [22]. Also with the conservative BBN bounds and particularly for $\epsilon_{\text{em}} \approx E_{\tau}$, such scenarios were believed to be almost completely excluded as can be seen in Fig. 16. With our update of the hadronic BBN constraints and the yield $Y_{\tilde{\tau}}^{m_{\tilde{\tau}_1} \ll m_{\tilde{e}_1, \tilde{\mu}_1}}$ given in (6.1), we find that superWIMP gravitino dark matter scenarios can be realized around the point D_1 : $(m_{\tilde{G}}, m_{\tilde{\tau}}) = (200 \text{ GeV}, 2.8 \text{ TeV})$ within the grey region and above the solid (red) hadronic exclusion limit. Here, however, one should keep in mind that hadronic tau decays could lead to additional constraints when the stau NLSP lifetime approaches 100 s. If the severe BBN bounds are too aggressive and the conservative ones are confirmed, superWIMP scenarios will also become allowed within the grey band around the point E_1 : $(m_{\tilde{G}}, m_{\tilde{\tau}}) = (450 \text{ GeV}, 1.2 \text{ TeV})$, i.e., below the solid (red) exclusion limit and above the dashed (blue) exclusion limit. In both of these allowed regions, superWIMP gravitino dark matter behaves as warm dark matter (see Fig. 14) and could resolve the small-scale structure problems of cold dark matter as suggested in Refs. [58, 59].

From a comparison of the BBN constraints shown in the left plot with the ones shown in the right plot of Fig. 16, one finds a strong sensitivity of the mass bounds on the upper limits $\xi_{\text{em, had}}^{\text{max}}$ shown in Fig. 9. For example, constraints obtained from the severe upper limits on ξ_{em} (almost completely) exclude scenarios with lifetimes $\tau_{\tilde{\tau}} \gtrsim 10^7$ s. In contrast, even significantly larger lifetimes remain allowed with the conservative upper limits on ξ_{em} . Since the upper limits on late energy injection $\xi_{\text{em, had}}^{\text{max}}$ depend strongly on the observed abundances of the primordial light elements, more precise determinations of these abundances will be crucial for future refinements of the exclusion limits.

Note that additional CMB constraints have been extracted from the high precision spectral measurements of the Cosmic Background Explorer Far Infrared Absolute Spectrophotometer (COBE FIRAS) [75]. These measurements found a very precise Planck spectrum. Possible deviations from such a spectrum can be described by a Bose–Einstein distribution with a chemical potential for which $|\mu| < 9 \times 10^{-5}$ has been found [75]. Since late electromagnetic energy release can lead to spectral distortions, this upper limit on $|\mu|$ can be translated into an upper limit on ϵ_{em} [76]. For late decays of the stau NLSP into the gravitino LSP, constraints on $m_{\tilde{G}}$ and $m_{\tilde{\tau}}$ inferred from the analytic approximation of [76] were given in Refs. [21, 22]. Using a numerical treatment of the kinetic equations for the photon number density, these constraints have recently been updated [74] with the estimate $Y_{\tilde{\tau}}^{m_{\tilde{\tau}_1} \ll m_{\tilde{e}_1, \tilde{\mu}_1}}$ given in (6.1). For $\epsilon_{\text{em}} = E_{\tau}$ and $\epsilon_{\text{em}} = 0.3 E_{\tau}$, the resulting CMB constraints are similar to the corresponding electromagnetic BBN constraints shown in the right plot of Fig. 16. Only towards the region around $(m_{\tilde{G}}, m_{\tilde{\tau}}) = (200 \text{ GeV}, 0.5 \text{ TeV})$, the CMB constraint obtained with $\epsilon_{\text{em}} = E_{\tau}$ becomes slightly more severe than the corresponding conservative BBN limit. In particular, the ‘gap’ in the electromagnetic BBN constraint for $\epsilon_{\text{em}} = E_{\tau}$ is excluded by the CMB constraint for $\epsilon_{\text{em}} = E_{\tau}$. The electromagnetic BBN constraints obtained from the severe BBN bounds however are much more severe than the CMB limits. In conclusion, since the present CMB constraints reduce the allowed region of $(m_{\tilde{G}}, m_{\tilde{\tau}})$ values only slightly when the conservative BBN bounds are considered, these limits will not be discussed further in the remainder of this paper. The CMB limits would

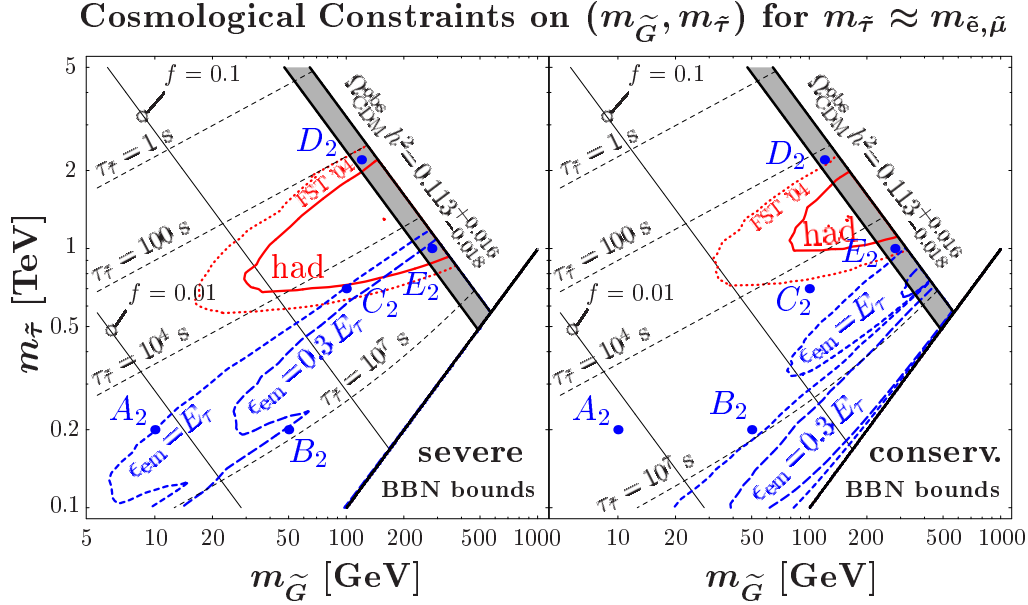


Figure 17: Same as Fig. 16 but for the stau NLSP abundance (6.2). The thick (blue) dots A_2 – E_2 indicate the benchmark scenarios that will be introduced in Sec. 9 (cf. Table 3).

become more important if an improved limit of $|\mu| < 2 \times 10^{-6}$ could be obtained in future missions such as the Absolute Radiometer for Cosmology, Astrophysics Diffuse Emission (ARCADE) or the Diffuse Microwave Emission Survey (DIMES) [74].

To illustrate the dependence of the mass bounds on the NLSP abundance, we extract now the bounds with the stau NLSP abundance (6.2) obtained for $m_{\tilde{\tau}_1} \approx m_{\tilde{e}_1, \tilde{\mu}_1}$, which is twice as large as the one considered in Fig. 16. The results are shown in Fig. 17. For the contours and exclusion limits, we use the same labels and plot styles as in Fig. 16. The thick (blue) dots indicate the benchmark scenarios A_2 – E_2 that will be introduced and discussed in Sec. 9. We find that the mass bounds in Fig. 17 have the same main features as the ones in Fig. 16. However, the region of allowed $(m_{\tilde{G}}, m_{\tilde{\tau}})$ values becomes smaller for the larger stau NLSP yield. Moreover, the allowed regions for superWIMP gravitino dark matter scenarios move to smaller values of $m_{\tilde{G}}$ and $m_{\tilde{\tau}}$, i.e., to the regions around the point D_2 : $(m_{\tilde{G}}, m_{\tilde{\tau}}) = (120 \text{ GeV}, 2.2 \text{ TeV})$ and the point E_2 : $(m_{\tilde{G}}, m_{\tilde{\tau}}) = (280 \text{ GeV}, 1 \text{ TeV})$. The latter of these will only be allowed for the conservative BBN bounds, i.e., if the severe BBN bounds turn out to be overly restrictive.

Note that thermal gravitino production can only contribute a negligible amount to the relic gravitino density in a superWIMP gravitino dark matter scenario with $\Omega_{\tilde{G}}^{\text{NTP}} \approx \Omega_{\text{CDM}}^{\text{obs}}$. Thus, for such a superWIMP gravitino dark matter scenario, the upper limits on the reheating temperature become severe; see Sec. 7. However, in most of the allowed region of $(m_{\tilde{G}}, m_{\tilde{\tau}})$ values, gravitinos from NLSP decays provide only a small fraction of $\Omega_{\text{CDM}}^{\text{obs}}$ so that thermally produced gravitinos can be the dominant component of cold dark matter.

At future colliders, one might be able to identify the point in the $(m_{\tilde{G}}, m_{\tilde{\tau}})$ plane realized in nature. Such prospects and associated implications for cosmology and particle physics will be described in Sec. 8. Already before the advent of new collider data, we find

upper bounds on the gravitino mass $m_{\tilde{G}}$ of about (100 – 300) GeV and (400 – 700) GeV from the exclusion limits in Figs. 16 and 17 respectively. These bounds can be refined and possibly tightened by computing the precise value of ϵ_{em} and by extending our study to smaller stau NLSP lifetimes. This is an important task since an upper limit on $m_{\tilde{G}}$ constrains the SUSY breaking scale which is crucial for insights into the SUSY breaking mechanism.

6.3 Mass Bounds for Gravitino Dark Matter Fractions from Slepton NLSP Decays

We now consider the mass bounds in scenarios in which a fixed fraction f of the observed amount of dark matter consists of gravitinos from late decays of charged slepton NLSPs. Such scenarios require an NLSP yield prior to decay of

$$Y_{\text{NLSP}} = f \frac{\Omega_{\text{CDM}}^{\text{obs}} h^2}{m_{\tilde{G}}} \frac{\rho_c}{s(T_0) h^2} = 4.1 \times 10^{-12} f \left(\frac{\Omega_{\text{CDM}}^{\text{obs}} h^2}{0.113} \right) \left(\frac{100 \text{ GeV}}{m_{\tilde{G}}} \right), \quad (6.3)$$

so that the bound from $\Omega_{\text{CDM}}^{\text{obs}}$ is respected by definition; see also Fig. 13. Accordingly, one is in the allowed region whenever the $\Omega_{\text{CDM}}^{\text{obs}}$ constraints are more severe than the BBN constraints shown in Fig. 12. Note that the abundance (6.3) depends only on $m_{\tilde{G}}$ for a given f . In contrast, the estimates of the thermal relic abundance given in (6.1) and (6.2) depend on $m_{\tilde{\tau}}$ but are independent of $m_{\tilde{G}}$. Indeed, only if the abundance (6.3) agrees with the estimates of the thermal relic abundance, will we consider it to be in a natural range.

In Fig. 18 we show the exclusion limits on $m_{\tilde{G}}$ and $m_{\tilde{\tau}}$ obtained when (6.3) with $f = 1, 0.1, \text{ and } 0.01$ (from top to bottom) is confronted with the severe (left) and conservative (right) BBN bounds for late ($\tau_{\tilde{\tau}} \gtrsim 100 \text{ s}$) NLSP decays. Contours of $\tau_{\tilde{\tau}}$ are also shown. For the BBN constraints and the $\tau_{\tilde{\tau}}$ contours, we use the labels and plot styles used already in Figs. 16 and 17. The allowed region is the one to the left of the curves from electromagnetic energy release (thick dashed lines, blue) and outside of the parameter region bounded by the curves from hadronic energy release (thick solid lines, red). Recall however that we consider scenarios with $\tau_{\tilde{\tau}} \gtrsim 100 \text{ s}$ and that additional constraints can appear for $\tau_{\tilde{\tau}} \lesssim 100 \text{ s}$. The grey bands indicate the regions in which the corresponding NLSP abundance (6.3) seems natural as it falls between the estimates of the thermal relic abundance given in (6.1) and (6.2). The exclusion limits inside the grey bands therefore resemble the ones found in Figs. 16 and 17. Above the grey bands, the abundance (6.3) becomes smaller than $Y_{\tilde{\tau}}^{m_{\tilde{\tau}_1} \ll m_{\tilde{e}_1, \tilde{\mu}_1}}$ so that $(m_{\tilde{G}}, m_{\tilde{\tau}})$ values are allowed that should be excluded according to Fig. 16. Below the grey bands, the abundance (6.3) becomes larger than $Y_{\tilde{\tau}}^{m_{\tilde{\tau}_1} \approx m_{\tilde{e}_1, \tilde{\mu}_1}}$ so that the BBN constraints exclude $(m_{\tilde{G}}, m_{\tilde{\tau}})$ values in Fig. 18 which are allowed in Fig. 17. For the considered scenarios, one sees clearly the increase of the allowed $(m_{\tilde{G}}, m_{\tilde{\tau}})$ region with decreasing f . Moreover, the dotted (red) lines show that the hadronic BBN constraints were overestimated towards large values of $m_{\tilde{\tau}}$ and underestimated towards small values of $m_{\tilde{\tau}}$ by the previous ϵ_{had} estimate of Ref. [21]. This is exactly the failure of the simplified treatment expected from Fig. 8.

Cosmological Constraints on $(m_{\tilde{G}}, m_{\tilde{\tau}})$ for $\Omega_{\tilde{G}}^{\text{NTP}} = f \Omega_{\text{CDM}}^{\text{obs}}$

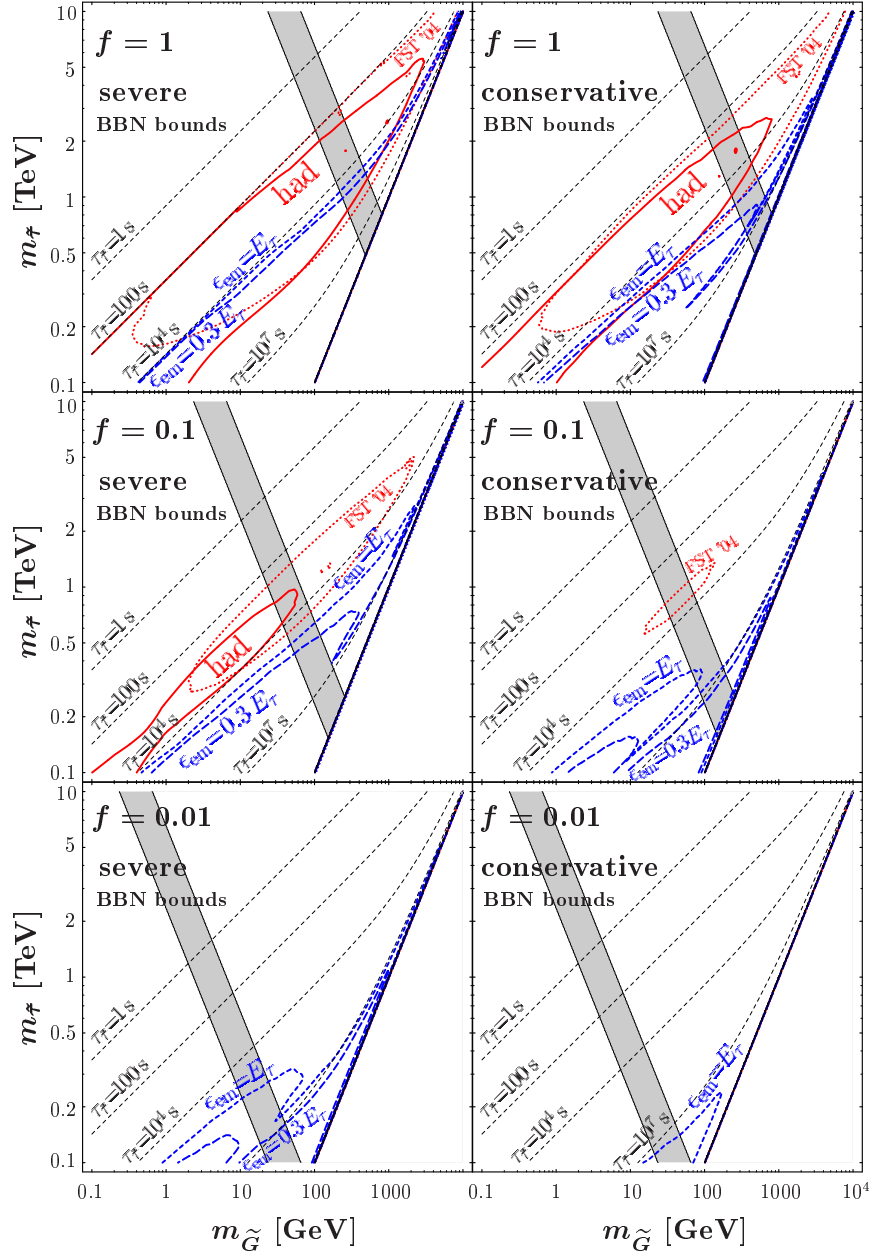


Figure 18: Exclusion limits for $m_{\tilde{G}}$ and $m_{\tilde{\tau}}$ from the severe (left) and conservative (right) BBN bounds on electromagnetic and hadronic energy release for scenarios in which gravitinos from stau NLSP decays provide 100%, 10%, and 1% of $\Omega_{\text{CDM}}^{\text{obs}}$ (from top to bottom). For the BBN constraints and the $\tau_{\tilde{\tau}}$ contours, we use the same labels and plot styles as in Fig. 16. Allowed is the region to the left of the thick dashed curve(s) and outside of the area enclosed by the thick solid curve. On the grey band, the stau NLSP abundance (6.3) has a natural value bounded by (6.1) and (6.2).

7. Gravitino Dark Matter from Thermal Production

In this section we consider the thermal production of gravitinos in the early Universe. We

compute the present free-streaming velocity and the comoving free-streaming scale of thermally produced gravitinos. We present upper limits on the reheating temperature after inflation, T_R , for scenarios in which a given fraction of the observed dark matter comprises of gravitinos from thermal production. We stress that these limits can be tightened by the cosmological constraints discussed in the previous sections. To illustrate the significance of the T_R bounds, we address the implications for thermal leptogenesis in a SUSY framework. A similar discussion can be found in the framework of the CMSSM with a gravitino LSP [23]. In our study we are exploring a wide range of the gravitino mass, the slepton NLSP mass, and the gluino mass, and we do not restrict our investigation to a constrained framework.

7.1 Relic Gravitino Density from Thermal Production in the Early Universe

Because of their extremely weak interactions, the temperature T_f at which gravitinos decouple from the thermal plasma can be very high depending on the gravitino mass. For $m_{\tilde{G}} \gtrsim 10$ keV (10 MeV), one finds a gravitino decoupling temperature of $T_f \gtrsim 100$ TeV (10^8 TeV). However, for a reheating temperature above the decoupling temperature, $T_R \gtrsim T_f$, the relic density of a gravitino LSP with 10 keV $\lesssim m_{\tilde{G}} \lesssim 1$ TeV exceeds $\Omega_{\text{CDM}}^{\text{obs}}$ significantly for any reasonable value of $g_{*S}(T_f)$ such as $g_{*S}(T_f) \simeq 230$, as can be seen from (5.9). Thus, only gravitino LSP scenarios with $T_R \ll T_f$ are allowed for 10 keV $\lesssim m_{\tilde{G}} \lesssim 1$ TeV.

Note that a light gravitino LSP with $m_{\tilde{G}} \simeq 100$ eV has a much smaller decoupling temperature of $T_f = \mathcal{O}(1$ TeV). For $T_R \gtrsim T_f$, such a gravitino—once in thermal equilibrium—would even provide the right amount of dark matter as can be seen from (5.9) with $g_{*S}(T_f) \simeq 100$. However, the velocity dispersion of such a light gravitino given by (5.10) exceeds significantly the constraints from observations and simulations of cosmic structures listed in Table 1.

For $T_R \ll T_f$, gravitinos can be produced in thermal reactions in the hot MSSM plasma. The thermal gravitino production rate at high temperatures is computed in a gauge-invariant way [16] with the Braaten–Yuan prescription [77] and hard thermal loop resummation [78], which takes into account Debye screening in the plasma. Assuming that inflation has diluted away any primordial gravitino abundance, gravitino disappearance processes are negligible for $T_R \ll T_f$. The corresponding Boltzmann equation can be solved analytically. To leading order in the gauge coupling of quantum chromodynamics, this leads to the following result for the relic density of stable LSP gravitinos from thermal production (TP) [16]

$$\Omega_{\tilde{G}}^{\text{TP}} h^2 = 0.12 g^2 \ln\left(\frac{1.163}{g}\right) \left(1 + \frac{m_{\tilde{g}}^2}{3m_{\tilde{G}}^2}\right) \left(\frac{m_{\tilde{G}}}{100 \text{ GeV}}\right) \left(\frac{T_R}{10^{10} \text{ GeV}}\right), \quad (7.1)$$

where g is the strong coupling and $m_{\tilde{g}}$ the gluino mass. The contribution proportional to $m_{\tilde{g}}^2$ results from the spin-1/2 components of the gravitino. Indeed, this contribution governs $\Omega_{\tilde{G}}^{\text{TP}} h^2$ for $m_{\tilde{G}} \ll m_{\tilde{g}}$. For larger values of the gravitino mass, $m_{\tilde{G}} \gtrsim 0.5 m_{\tilde{g}}$, the contribution of the spin-3/2 components—which is independent of $m_{\tilde{g}}$ —becomes equally important.

Gravitino Density from Thermal Production

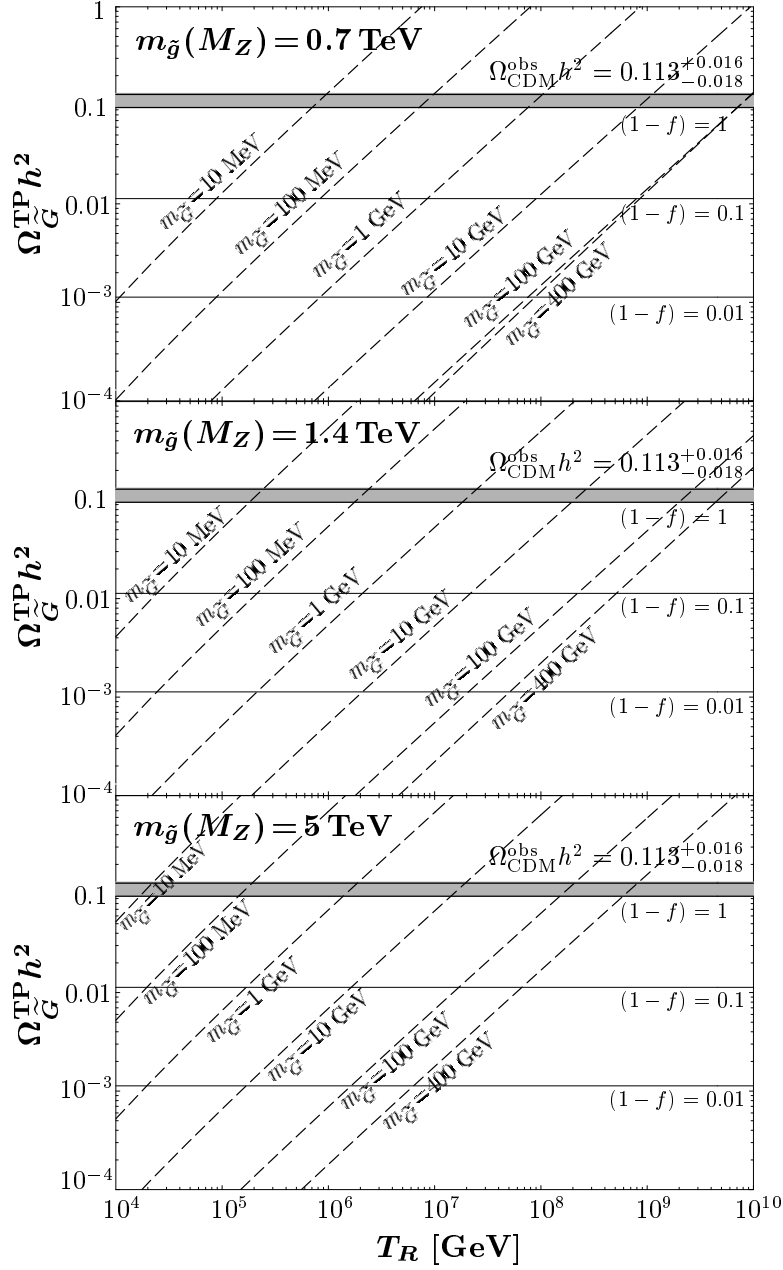


Figure 19: The relic density of gravitino LSPs from thermal production, $\Omega_{\tilde{G}}^{\text{TP}} h^2$, as a function of T_R for $m_{\tilde{g}}(M_Z) = 0.7$ TeV (top), 1.4 TeV (middle), and 5 TeV (bottom). The dashed lines show the results for $m_{\tilde{G}} = 10$ MeV, 100 MeV, 1 GeV, 10 GeV, 100 GeV, and 400 GeV (from the upper left to the lower right). The grey band indicates the observed dark matter density $\Omega_{\text{CDM}}^{\text{obs}} h^2 = 0.113^{+0.016}_{-0.018}$ (95% CL) [52, 7]. On the solid lines labeled with $(1-f) = 0.1$ and $(1-f) = 0.01$, the contribution of thermally produced gravitinos to $\Omega_{\text{CDM}}^{\text{obs}}$ is 10% and 1% respectively.

In Fig. 19 the dashed lines show $\Omega_{\tilde{G}}^{\text{TP}} h^2$ as a function of the reheating temperature T_R for different values of the gravitino mass $m_{\tilde{G}}$ ranging from 10 MeV to 400 GeV (from

the upper left to the lower right), where the values $m_{\tilde{g}}(M_Z) = 0.7$ TeV (top), 1.4 TeV (middle), and 5 TeV (bottom) are considered. The running of the strong coupling and the gluino mass is taken into account by replacing g and $m_{\tilde{g}}$ in (7.1) respectively with $g(T_R) = [g^{-2}(M_Z) + 3 \ln(T_R/M_Z)/(8\pi^2)]^{-1/2}$ and $m_{\tilde{g}}(T_R) = [g(T_R)/g(M_Z)]^2 m_{\tilde{g}}(M_Z)$, where $g^2(M_Z)/(4\pi) = 0.118$. The upper two plots show explicitly that a doubling of the gluino mass enhances $\Omega_{\tilde{G}}^{\text{TP}} h^2$ by a factor of four for $m_{\tilde{G}} \ll m_{\tilde{g}}$. The results obtained for $m_{\tilde{G}} = 400$ GeV demonstrate that the contribution of the spin-3/2 components becomes important for $m_{\tilde{G}} \gtrsim 0.5 m_{\tilde{g}}$. On the grey band, $\Omega_{\tilde{G}}^{\text{TP}}$ agrees with $\Omega_{\text{CDM}}^{\text{obs}}$. On the solid lines labeled with $(1-f) = 0.1$ and $(1-f) = 0.01$, the thermally produced gravitinos provide respectively 10% and 1% of $\Omega_{\text{CDM}}^{\text{obs}}$, which leaves room for a significant contribution of gravitinos from stau NLSP decays.

In studies of scenarios with gravitino LSP and stau NLSP, a gluino mass above the mass of the lighter stau has to be considered. For such scenarios, one should also keep in mind that a gravitino LSP with $m_{\tilde{G}} \gtrsim 10$ GeV can be excluded for certain values of the stau NLSP mass by the cosmological constraints shown in Figs. 16 and 17. In particular, gravitino masses above about 700 GeV seem to be excluded for any value of the stau NLSP mass as stressed at the end of Sec. 6.2.

7.2 Free Streaming of Gravitinos from Thermal Production

For a reheating temperature below the gravitino decoupling temperature, gravitinos have never been in thermal equilibrium with the primordial plasma. However, since the thermal production proceeds through reactions of particles in thermal equilibrium, the gravitinos are produced in kinetic equilibrium with the primordial plasma. Therefore, the gravitinos from thermal production have a thermal spectrum. The root mean squared value of their velocity dispersion today is accordingly given by

$$(v_{\text{FS}}^{\text{rms},0})^{\tilde{G}\text{TP}} = 5.8 \times 10^{-6} \frac{\text{km}}{\text{s}} \left(\frac{10 \text{ MeV}}{m_{\tilde{G}}} \right) \left(\frac{230}{g_{*S}(T_R)} \right)^{1/3}. \quad (7.2)$$

Since the thermal gravitino production is efficient only in the very early hot Universe, the corresponding comoving free-streaming scale can be estimated from expression (5.6) with $v_0 = (v_{\text{FS}}^{\text{rms},0})^{\tilde{G}\text{TP}}$. Thermally produced gravitino LSPs with $m_{\tilde{G}} \gtrsim 100$ keV have a negligible free-streaming behavior and thus can be classified as cold dark matter. Accordingly, in scenarios in which basically all dark matter is made of such gravitinos, one must face the small-scale ($\lesssim 1$ Mpc) structure problems inherent to cold dark matter models.

7.3 Upper Limits on the Reheating Temperature

Since $\Omega_{\tilde{G}}^{\text{TP}}$ depends on the reheating temperature after inflation, the observed dark matter density allows us to extract upper limits on T_R as a function of $m_{\tilde{G}}$ in gravitino LSP scenarios with a given gluino mass [11, 15, 16, 23, 25]. These limits will become particularly severe if $m_{\tilde{g}} \gg m_{\tilde{G}}$ and if gravitinos from NLSP decays provide already a sizeable fraction f of $\Omega_{\text{CDM}}^{\text{obs}}$. The range of allowed values of the reheating temperature is crucial for our

understanding of inflation. Moreover, thermal leptogenesis provides an attractive explanation of the baryon asymmetry in the Universe for very high reheating temperatures of $T_R \gtrsim 3 \times 10^9$ GeV [47, 48].

In Fig. 20 we show the reheating temperatures T_R for which $\Omega_{\tilde{G}}^{\text{TP}} = (1 - f) \Omega_{\text{CDM}}^{\text{obs}}$ with $(1 - f) = 1, 0.1,$ and 0.01 (as labeled) as a function of $m_{\tilde{G}}$. The results are presented for gluino masses of $m_{\tilde{g}}(M_Z) = 0.7$ TeV (top), 1.4 TeV (middle), and 5 TeV (bottom). Since our focus is on gravitino LSP scenarios, we consider only gravitino masses that are smaller than the running gluino mass. For the $(m_{\tilde{G}}, T_R)$ values within the grey band, $\Omega_{\tilde{G}}^{\text{TP}}$ agrees with the observed dark matter density $\Omega_{\text{CDM}}^{\text{obs}}$. The region above the grey band is excluded for any value of the NLSP mass. If the NLSP decays provide already 90% or 99% of $\Omega_{\text{CDM}}^{\text{obs}}$, we can exclude the region above the solid lines labeled respectively with $(1 - f) = 0.1$ or $(1 - f) = 0.01$. Also the $m_{\tilde{G}}$ bounds presented for charged slepton NLSP scenarios in Figs. 16 and 17 can tighten the T_R limits for $m_{\tilde{G}} \gtrsim 10$ GeV, even in scenarios with $f \ll 1$. We use again thick dots to indicate the benchmark scenarios $A_{(1,2)}-E_{(1,2)}$ (red, blue) that will be introduced and discussed in Sec. 9.

Figure 20 shows that thermal leptogenesis cannot explain the observed value of the baryon asymmetry in a SUSY framework with gravitino LSP and a heavy gluino $m_{\tilde{g}}(M_Z) = 5$ TeV. Similar investigations have found that successful thermal leptogenesis ($T_R \gtrsim 3 \times 10^9$ GeV) implies upper bounds on the gluino mass of about 1.3 TeV and 1.8 TeV respectively for charged slepton NLSP and sneutrino NLSP scenarios [19]. We postpone an update of the gluino mass bounds based on our improved cosmological constraints for future work.

8. Prospects for Collider Phenomenology and Cosmology

In this section we describe the possible interplay between astrophysical investigations and studies at future particle accelerators—such as the Large Hadron Collider (LHC) and the International Linear Collider (ILC)—for gravitino LSP scenarios with a charged slepton NLSP. We review potential collider signatures of gravitino dark matter and stress the implications for cosmology.

For phenomenology at future colliders, the SUSY scenario with a charged slepton NLSP and an extremely weakly interacting LSP such as the gravitino is particularly promising [36, 37, 38, 39, 40, 41, 42, 22, 43, 44, 45, 25]. Because of its long lifetime, the charged slepton NLSP would appear as a (quasi-)stable particle. Such a long-lived heavy charged particle would penetrate collider detectors in a way similar to muons [36, 37, 39]. A significant fraction of the NLSP decays will take place outside the detector and will thus escape detection. If the produced charged slepton NLSPs are slow, the associated highly ionizing tracks and time-of-flight measurements will allow one to distinguish the NLSP sleptons from muons [36, 37, 39, 41]. From measurements of the velocity $\beta_{\tilde{1}} \equiv v_{\tilde{1}}/c$ and the momentum $p_{\tilde{1}} \equiv |\vec{p}_{\tilde{1}}|$ of the long-lived slepton, its mass can be determined from the standard relation $m_{\tilde{1}} = p_{\tilde{1}} \sqrt{1 - \beta_{\tilde{1}}^2} / \beta_{\tilde{1}}$ [41]. If some of the charged slepton NLSPs would decay already in the detectors, the statistical method proposed in Ref. [41] could allow one to measure the lifetime of the slepton NLSP. Since this lifetime is governed by the 2-body

Upper Limits on the Reheating Temperature

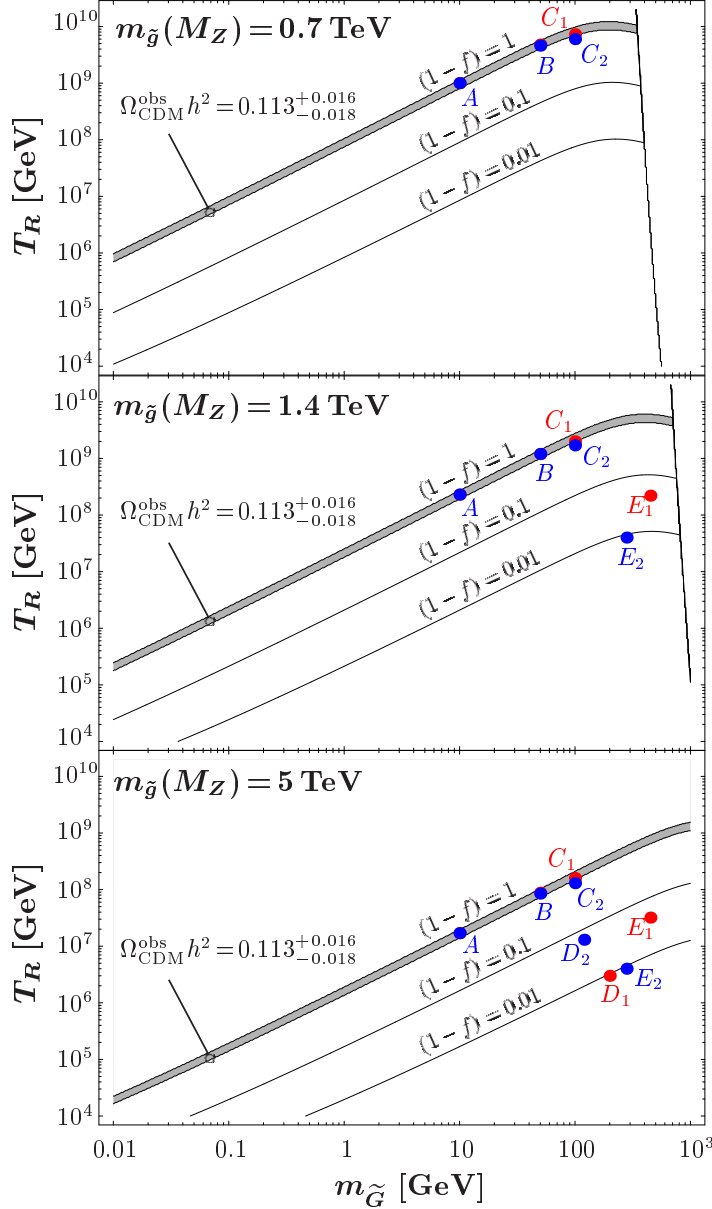


Figure 20: The reheating temperatures T_R for which thermally produced gravitino LSPs provide 100% (grey band), 10% (middle solid line), and 1% (lower solid line) of $\Omega_{\text{CDM}}^{\text{obs}} h^2 = 0.113_{-0.018}^{+0.016}$ (95% CL) [52, 7], where $m_{\tilde{g}}(M_Z) = 0.7$ TeV (top), 1.4 TeV (middle), and 5 TeV (bottom). The region above the grey band is excluded for any value of the NLSP mass. For a given superparticle spectrum, an additional upper bound on $m_{\tilde{G}}$ is obtained which can lead to a more severe upper limit on T_R ; see Figs. 16 and 17 for stau NLSP scenarios. The thick dots indicate the benchmark scenarios $A_{(1,2)}-E_{(1,2)}$ (red, blue) that will be introduced in Sec. 9 (cf. Tables 2 and 3).

decay $\tilde{l} \rightarrow \tilde{G}l$ in the gravitino LSP case, we can use the decay rate (2.2) with the measured value of $m_{\tilde{l}}$ to determine also the gravitino mass $m_{\tilde{G}}$. This would be an experimental determination of the $(m_{\tilde{G}}, m_{\tilde{l}})$ point in Figs. 16 and 17.

In addition, there have been works, which propose ways to stop and collect charged long-lived particles for an analysis of their decays [79, 43, 44]. It was found that up to $\mathcal{O}(10^3\text{--}10^4)$ and $\mathcal{O}(10^3\text{--}10^5)$ of charged slepton NLSPs can be trapped per year at the LHC and the ILC, respectively, by placing 1–10 kt of massive additional material around planned collider detectors [43, 44]. With $\mathcal{O}(10^4)$ of analyzed NLSP decays, one could distinguish between the gravitino LSP scenario and the alternative axino LSP scenario by considering the differential distributions of the visible decay products in the 3-body decay of the slepton NLSP into the LSP, the corresponding lepton, and a photon [45, 25]. The axino is another extremely weakly interacting LSP candidate, which can also be produced in decays of charged slepton NLSPs [80, 45, 25] and in thermal reactions in the very early Universe [81, 82]. In the axino LSP case, the analysis of the slepton NLSP decays could allow one to determine the axino mass and to estimate the Peccei–Quinn scale [45, 25]. In the gravitino LSP case, $m_{\tilde{G}}$ could be inferred kinematically. If so, one will be able to use the decay rate (2.1) to determine the Planck scale M_{Pl} microscopically from the measured slepton NLSP lifetime and the measured values of $m_{\tilde{G}}$ and $m_{\tilde{\tau}}$. If consistent with macroscopic measurements of M_{Pl} , this will be strong evidence for the existence of SUGRA in nature [42].

The prospects for phenomenology with long-lived charged NLSP sleptons at future colliders depend strongly on the mass spectrum of the superpartners. The heavier the superparticles the smaller will be the total SUSY production cross section and, in particular, the charged slepton NLSP production cross section. If $m_{\tilde{\tau}}$ is smaller than about 0.2 TeV, the charged slepton NLSP will be copiously produced in the proton–proton collisions of c.m. energy $\sqrt{s} = 14$ TeV at the LHC and even in the electron–positron collisions of c.m. energy $\sqrt{s} = 0.5$ TeV at the ILC. A long-lived charged slepton NLSP with $m_{\tilde{\tau}} = 0.7$ TeV could possibly still be discovered at the LHC with a luminosity of 100 fb^{-1} [22]. At the ILC this will require the second phase in which a c.m. energy of $\sqrt{s} = 1$ TeV might be reached. Heavier NLSPs will be difficult to explore at the LHC since the production rate becomes very small. Even smaller production rates are expected at the ILC; cf. [22, 43, 44] and references therein.

The appearance of a long-lived charged slepton as the lightest standard model superpartner in the collider detector would already be a strong hint towards physics beyond the MSSM. Indeed, from the severe constraints for stable charged massive particles (cf. [83] and references therein), one would expect that the charged slepton will eventually decay. A long-lived charged slepton thus points to an extremely weakly interacting LSP such as the gravitino or the axino.

Once the mass of the long-lived slepton is measured, the cosmological constraints shown in Figs. 16 and 17 at the measured value of $m_{\tilde{\tau}}$ could tighten the upper bound on the gravitino mass discussed at the end of Sec. 6.2. This upper bound on $m_{\tilde{G}}$, which implicitly assumes the gravitino LSP scenario, will imply an upper bound for the SUSY breaking scale. In addition, this $m_{\tilde{G}}$ constraint will give an upper limit on the amount of dark matter that could come from late decays of the charged NLSP sleptons. If it turns out that this amount is only a minor fraction ($f \lesssim 0.1$) of the observed dark matter density, there will be room for a significant contribution of thermally produced gravitino

dark matter and, thus, for high values of the reheating temperature.

If one succeeds to analyze the decays of the long-lived sleptons and to find evidence for the gravitino LSP, this will provide an experimental determination of the $(m_{\tilde{G}}, m_{\tilde{\tau}})$ point as described above. The obtained values of $m_{\tilde{G}}$ and $m_{\tilde{\tau}}$ will then fix the maximum amount of gravitino dark matter from slepton NLSP decays. Since the remaining fraction of the dark matter density can be made of thermally produced gravitinos, this will give an upper limit on the reheating temperature after inflation, which is crucial for our understanding of inflation and the baryon asymmetry of the Universe. At this point, it will also be interesting to see whether the obtained $(m_{\tilde{G}}, m_{\tilde{\tau}})$ point falls into the region which we expect to be allowed by the cosmological constraints shown in Figs. 16 and 17.

We expect that the cosmological constraints can be refined with future astrophysical investigations and insights from future colliders. By reducing the uncertainties in the observed abundances of the light primordial elements and by improving the numerical studies of the effects of late decaying particles on those elements, one should be able to reduce the uncertainty between the limits from the severe and the conservative BBN bounds shown in Figs. 16 and 17. If the masses of the lightest SUSY particles and their couplings can be determined at future colliders, one will also be able to compute the yield of the slepton NLSP before its decay with high precision, particularly, for the scenario in which the slepton NLSPs were once in thermal equilibrium. Such a precise determination of Y_{NLSP} will reduce the uncertainty between the constraints shown in Fig. 16 and the ones shown in Fig. 17. Experimental insights into the mass hierarchy of the lightest superpartners can also be necessary in order to calculate reliably the electromagnetic energy release ϵ_{em} and the associated exclusion limits.

9. Benchmark Scenarios with Gravitino LSP and Stau NLSP

To summarize the insights gained from the cosmological constraints presented above, we consider ten benchmark scenarios $A_{1,2}$ to $E_{1,2}$ for the case of the gravitino LSP and the stau NLSP with $m_{\tilde{G}}$ not smaller than 10 GeV and $m_{\tilde{B}} = 1.1 m_{\tilde{\tau}}$. We present the scenarios A_1 to E_1 for $m_{\tilde{\tau}_1} \ll m_{\tilde{e}_1, \tilde{\mu}_1}$ in Table 2 and the scenarios A_2 to E_2 for $m_{\tilde{\tau}_1} \approx m_{\tilde{e}_1, \tilde{\mu}_1}$ in Table 3. Each scenario is given by $(m_{\tilde{G}}, m_{\tilde{\tau}})$ with $m_{\tilde{\tau}_1} \ll m_{\tilde{e}_1, \tilde{\mu}_1}$ or $m_{\tilde{\tau}_1} \approx m_{\tilde{e}_1, \tilde{\mu}_1}$ and represented respectively by a thick (red) dot in Fig. 16 or by a thick (blue) dot in Fig. 17. We also use thick (red, blue) dots to indicate the benchmark points $A_{1,2}$ – $E_{1,2}$ in Fig. 20. In the tables, we list for each scenario the lifetime of the stau NLSP $\tau_{\tilde{\tau}}$, the fraction f of $\Omega_{\text{CDM}}^{\text{obs}}$ which is provided by gravitinos from stau NLSP decays, the present velocity dispersion of such non-thermally produced gravitinos $(v_{\text{FS}}^0)^{\tilde{G}^{\text{NTP}}}$, and an associated classification as a hot, warm, or cold dark matter component. In addition, we indicate whether the severe and/or conservative BBN bounds are respected. We assume that the remaining fraction $(1 - f)$ of $\Omega_{\text{CDM}}^{\text{obs}}$ consists of thermally produced gravitinos and specify also the present velocity dispersion of the thermally produced gravitinos $(v_{\text{FS}}^0)^{\tilde{G}^{\text{TP}}}$ which allows us to classify this component as cold dark matter. Moreover, the reheating temperature T_R required for $\Omega_{\tilde{G}}^{\text{TP}} = (1 - f)\Omega_{\text{CDM}}^{\text{obs}}$ is given for gluino masses of $m_{\tilde{g}}(M_Z) = 0.7 \text{ TeV}$, 1.4 TeV , and 5.0 TeV . Note that higher values of T_R are excluded while lower values of T_R are

Table 2: Benchmark scenarios for the gravitino LSP and stau NLSP case with $m_{\tilde{\tau}_1} \ll m_{\tilde{e}_1, \tilde{\mu}_1}$.

Scenario	A_1	B_1	C_1	D_1	E_1
$m_{\tilde{G}}$ [GeV]	10	50	100	200	450
$m_{\tilde{\tau}}$ [TeV]	0.2	0.2	0.7	2.8	1.2
$\tau_{\tilde{\tau}}$ [s]	1.9×10^5	6.0×10^6	3.8×10^4	140	8.8×10^4
conservative BBN bounds	yes	yes	yes	yes (?)	yes
severe BBN bounds	yes	? (ϵ_{em})	yes	yes (?)	no
f	3.5×10^{-3}	1.8×10^{-2}	0.12	0.99	0.96
$(v_{\text{FS}}^0)^{\tilde{G} \text{ NTP}}$ [km/s]	0.26	0.28	0.04	0.005	0.02
	hot	hot	warm	warm	warm
$(v_{\text{FS}}^{\text{rms},0})^{\tilde{G} \text{ TP}}$ [km/s]	5.8×10^{-9}	1.2×10^{-9}	5.8×10^{-10}	2.9×10^{-10}	1.3×10^{-10}
	cold	cold	cold	cold	cold
$T_R^{m_{\tilde{g}}=0.7 \text{ TeV}}$ [GeV]	1.0×10^9	4.8×10^9	7.3×10^9	–	–
$T_R^{m_{\tilde{g}}=1.4 \text{ TeV}}$ [GeV]	2.3×10^8	1.2×10^9	2.0×10^9	–	2.2×10^8
$T_R^{m_{\tilde{g}}=5.0 \text{ TeV}}$ [GeV]	1.7×10^7	8.8×10^7	1.6×10^8	3.0×10^6	3.2×10^7

Table 3: Benchmark scenarios for the gravitino LSP and stau NLSP case with $m_{\tilde{\tau}_1} \approx m_{\tilde{e}_1, \tilde{\mu}_1}$.

Scenario	A_2	B_2	C_2	D_2	E_2
$m_{\tilde{G}}$ [GeV]	10	50	100	120	280
$m_{\tilde{\tau}}$ [TeV]	0.2	0.2	0.7	2.2	1.0
$\tau_{\tilde{\tau}}$ [s]	1.9×10^5	6.0×10^6	3.8×10^4	140	8.8×10^4
conservative BBN bounds	yes	yes	yes	yes (?)	yes
severe BBN bounds	yes	? (ϵ_{em})	yes	yes (?)	no
f	7.1×10^{-3}	3.3×10^{-2}	0.25	0.93	0.99
$(v_{\text{FS}}^0)^{\tilde{G} \text{ NTP}}$ [km/s]	0.26	0.28	0.04	0.005	0.02
	hot	hot	warm	warm	warm
$(v_{\text{FS}}^{\text{rms},0})^{\tilde{G} \text{ TP}}$ [km/s]	5.8×10^{-9}	1.2×10^{-9}	5.8×10^{-10}	2.9×10^{-10}	1.3×10^{-10}
	cold	cold	cold	cold	cold
$T_R^{m_{\tilde{g}}=0.7 \text{ TeV}}$ [GeV]	1.0×10^9	4.6×10^9	6.0×10^9	–	–
$T_R^{m_{\tilde{g}}=1.4 \text{ TeV}}$ [GeV]	2.3×10^8	1.2×10^9	1.7×10^9	–	4.0×10^7
$T_R^{m_{\tilde{g}}=5.0 \text{ TeV}}$ [GeV]	1.7×10^7	8.5×10^7	1.3×10^8	1.3×10^7	4.0×10^6

possible with additional gravitino sources such as inflaton decays [26] and/or additional dark matter constituents such as axions [84]. Depending on the value of f , we can group the scenarios $A_{1,2}$ to $E_{1,2}$ into the three classes which are discussed in the following.

In the scenarios $A_{1,2}$ and $B_{1,2}$, the stau NLSP decays contribute less than 5% of the observed dark matter density. This minor fraction can be classified as hot dark matter as it has a relatively high velocity dispersion today, $(v_{\text{FS}}^0)^{\tilde{G} \text{ NTP}} > 0.2$ km/s. The dominant contribution to $\Omega_{\text{CDM}}^{\text{obs}}$ can thus consist of thermally produced gravitinos. These gravitinos have a negligible velocity dispersion today and thus can be classified as cold dark matter. Accordingly, the small-scale structure problems of cold dark matter remain to be resolved. Reheating temperatures of $T_R \gtrsim 10^9$ GeV will be allowed in these scenarios if the gluino mass is not much larger than 1 TeV. In particular, for the points $B_{1,2}$ and a gluino mass not much larger than 0.7 TeV, thermal leptogenesis provides a viable explanation of the

baryon asymmetry. The severe and conservative BBN bounds are respected by the points $A_{1,2}$. The points $B_{1,2}$ respect the conservative BBN bounds as well but will respect the severe BBN bounds only if $\epsilon_{\text{em}} \simeq 0.3 E_\tau$. For a larger electromagnetic energy release, the points $B_{1,2}$ will not be allowed by the severe BBN bounds. The appealing feature of the points $A_{1,2}$ and $B_{1,2}$ is the relatively low stau NLSP mass of $m_{\tilde{\tau}} = 0.2$ TeV, which would make these scenarios accessible at the LHC and also at the ILC already in its first phase with $\sqrt{s} = 0.5$ TeV. Note that the stau NLSP mass is only four times larger than the gravitino mass in the scenarios $B_{1,2}$. The spin-3/2 components of the gravitino emitted in the stau NLSP decay would therefore be non-negligible and even a measurement of the gravitino spin would be conceivable [42].

In the scenarios $C_{1,2}$, the gravitinos from stau NLSP decays provide a considerable fraction of about (10 – 25)% of the observed dark matter density. This fraction has a non-negligible velocity dispersion today, $(v_{\text{FS}}^0)^{\tilde{G}^{\text{NTP}}} > 0.04$ km/s, and can be classified as warm dark matter. If the remaining part of $\Omega_{\text{CDM}}^{\text{obs}}$ is made of thermally produced gravitinos, which would have a negligible velocity dispersion today, one will have mixed gravitino dark matter with a cold and a warm component. Again it is not clear at this point if the small-scale structure problems of cold dark matter can be overcome in such a scenario. However, such a scenario is clearly allowed by the severe and the conservative BBN constraints. At the points $C_{1,2}$, the reheating temperature needed for successful thermal leptogenesis, $T_R \gtrsim 3 \times 10^9$ GeV, will be allowed if the gluino mass is not much larger than 1 TeV. Note the exceptional case of a gluino with a mass of 0.7 TeV which would be as light as the stau NLSP. In this case, we implicitly assume a finite mass difference since the gluino NLSP scenario is excluded by hadronic BBN constraints [19]. A stau NLSP with a mass of $m_{\tilde{\tau}} = 0.7$ TeV will be very hard to produce in the LHC experiments and will be out of reach in the first phase of the ILC. However, as discussed in Sec. 8, even a small number of long-lived stau NLSPs could give an exciting signature and could allow us to determine the stau NLSP mass.

In the scenarios $D_{1,2}$ and $E_{1,2}$, more than 90% of the observed cold dark matter density is made of gravitinos from stau NLSP decays. The emitted gravitinos still have a non-negligible velocity dispersion today, $(v_{\text{FS}}^0)^{\tilde{G}^{\text{NTP}}} = 0.005 - 0.02$ km/s. As warm dark matter, they could explain the observed power on small scales, which is significantly lower than expected from simulations of cold dark matter. Since the contribution of the thermally produced gravitinos cannot exceed 10% of the observed dark matter density, the reheating temperature after inflation is constrained to values below about $T_R = 10^8$ GeV. Accordingly, thermal leptogenesis seems excluded as a possible explanation of the baryon asymmetry in these scenarios. However, it should be stressed that the scenarios $D_{1,2}$ and $E_{1,2}$ can be in conflict with the BBN bounds. In particular, the points $E_{1,2}$ are already excluded by the severe BBN bounds. The points $D_{1,2}$ seem to be allowed but these points are associated with stau NLSP lifetimes close to 100 s, where additional constraints could arise from hadronic decays of tau leptons. Unfortunately, the scenarios $D_{1,2}$ and $E_{1,2}$ will be extremely hard to probe at the LHC and impossible to probe at the ILC. A stau NLSP heavier than about 1 TeV implies that all standard model superpartners are heavier than about 1 TeV and, thus, a very small value of even the total SUSY production cross section.

Finally, we stress that scenarios with $m_{\tilde{G}} \lesssim 10$ GeV and $m_{\tilde{\tau}} \lesssim 5$ TeV cannot be excluded by the constraints from BBN and $\Omega_{\text{CDM}}^{\text{obs}}$. In this region of the parameter space, the contribution of gravitino dark matter from NLSP decays is below 10% of $\Omega_{\text{CDM}}^{\text{obs}}$ so that almost all of the observed amount of dark matter can be explained by thermally produced gravitinos. The upper bounds on the reheating temperature however become more severe towards smaller values of $m_{\tilde{G}}$ as shown in Fig. 20. Moreover, for $m_{\tilde{G}} \lesssim 100$ keV, the present velocity dispersion of thermally produced gravitinos becomes non-negligible so that these gravitinos can be classified as warm dark matter. The warm dark matter constraints listed in Table 1 can then be used to exclude thermally produced gravitinos with $m_{\tilde{G}} \lesssim 100$ eV.

10. Conclusions

We have presented a systematic and thorough investigation of cosmological constraints in R -parity respecting SUSY scenarios with a gravitino LSP and a long-lived ($\tau_{\tilde{1}} \gtrsim 100$ s) charged slepton NLSP. The gravitino appears naturally as the LSP in well-motivated SUSY breaking schemes [1, 3, 5] and the lighter stau as the lightest standard model superpartner in high-energy frameworks. Scenarios with the gravitino LSP and the stau NLSP are particularly promising: The gravitino LSP is a natural dark matter candidate and the long-lived stau NLSP could provide striking signatures at future colliders [36, 37, 38, 39, 40, 41] which could lead to experimental evidence for gravitino dark matter [42, 45, 25].

In our study we have assumed that gravitino dark matter originates from thermal production in the early Universe [11, 12, 14, 16] and from late NLSP decays [13, 15, 17, 18, 21, 22], both of which are guaranteed production mechanisms. We have examined the relic density of gravitinos, $\Omega_{\tilde{G}}$, their present free-streaming velocity, $v_{\text{FS}}^{\tilde{G}}$, the release of electromagnetic and hadronic energy in late decays of charged NLSP sleptons, $\epsilon_{\text{em,had}}$, and the yield of the NLSP sleptons before their decay, $Y_{\tilde{1}}$. These quantities are constrained by the observed dark matter density, by observations and simulations of cosmic structures, and by the observed abundances of the light primordial elements. We have used these cosmological constraints to extract bounds on the gravitino mass, $m_{\tilde{G}}$, the mass of the charged slepton NLSP, $m_{\tilde{1}}$, and the reheating temperature after inflation, T_R . In addition, upper limits on the yield of purely right-handed NLSP sleptons before their decay, $Y_{\tilde{1}}^{\text{max}}$, have been obtained.

New results for the hadronic energy release ϵ_{had} in late ($\tau_{\tilde{1}} \gtrsim 100$ s) decays of charged right-handed slepton NLSPs have been presented from our computation of the 4-body decay of the slepton NLSP into the gravitino, the corresponding lepton, and a quark–antiquark pair. In our computation, we have taken into account the exchange of virtual electroweak gauge bosons and the exact energy spectrum of the emitted quark–antiquark pair. In the previous estimate, only Z-boson exchange in the zero-width approximation was considered together with a simplified monochromatic approximation of the energy of the quark–antiquark pair [21]. From a comparison with our exact treatment, we find that ϵ_{had} has been underestimated towards smaller values of $m_{\tilde{\tau}}$ and overestimated for $m_{\tilde{\tau}} \gg m_{\tilde{G}}$. Therefore, the hadronic nucleosynthesis constraints given in Refs. [21, 22, 23], which were derived from the simplified estimate of Ref. [21], have to be updated.

With our exact computation of ϵ_{had} , we have derived new upper limits on $Y_{\tilde{\tau}_1}$ from the recent nucleosynthesis constraints on late energy injection, $\xi_{\text{em, had}} (\equiv \epsilon_{\text{em, had}} Y_{\tilde{\tau}_1})$, given in Ref. [29, 31]. We have applied the BBN bounds from the observed abundances of primordial D and ${}^4\text{He}$ since they are the most reliable ones. To account for the present uncertainties of these abundances, we have used one severe and one conservative BBN bound for both hadronic and electromagnetic energy injection. We find that the hadronic limits $Y_{\text{Ihad}}^{\text{max}}$ become serious for $m_{\tilde{G}} \gtrsim 100$ GeV and $m_{\tilde{\tau}} \gtrsim 0.7$ TeV, and already for NLSP lifetimes of $100 \text{ sec} < \tau_{\tilde{\tau}_1} < 10^4 \text{ sec}$. In contrast, the electromagnetic limits $Y_{\text{IEM}}^{\text{max}}$ can be important for smaller values of $m_{\tilde{G}}$ and $m_{\tilde{\tau}}$ but only for NLSP lifetimes of $\tau_{\tilde{\tau}_1} > 10^4 \text{ sec}$.

We have also discussed the upper limit on $Y_{\tilde{\tau}_1}$ from the observed dark matter density, $\Omega_{\text{CDM}}^{\text{obs}}$, which arises since the gravitino density from NLSP decays, $\Omega_{\tilde{G}}^{\text{NTP}}$, cannot exceed $\Omega_{\text{CDM}}^{\text{obs}}$. This upper limit $Y_{\text{ICDM}}^{\text{max}}$ is independent of $m_{\tilde{\tau}}$. It becomes severe towards larger values of $m_{\tilde{G}}$ and for scenarios in which the thermally produced gravitino density $\Omega_{\tilde{G}}^{\text{NTP}}$ dominates $\Omega_{\text{CDM}}^{\text{obs}}$.

The upper limits $Y_{\text{Iem}}^{\text{max}}$, $Y_{\text{Ihad}}^{\text{max}}$, and $Y_{\text{ICDM}}^{\text{max}}$ have allowed us to extract bounds on $m_{\tilde{G}}$ and $m_{\tilde{\tau}}$ for scenarios in which the NLSP sleptons freeze out with a thermal abundance. Since the thermal relic abundance of the slepton NLSP prior to decay is sensitive to the mass spectrum and the couplings of the superparticles, we have considered an estimate $Y_{\tilde{\tau}}^{m_{\tilde{\tau}_1} \ll m_{\tilde{e}_1, \tilde{\mu}_1}}$ for $m_{\tilde{\tau}_1} \ll m_{\tilde{e}_1, \tilde{\mu}_1}$ and another estimate $Y_{\tilde{\tau}}^{m_{\tilde{\tau}_1} \approx m_{\tilde{e}_1, \tilde{\mu}_1}}$ for $m_{\tilde{\tau}_1} \approx m_{\tilde{e}_1, \tilde{\mu}_1}$, where $Y_{\tilde{\tau}}^{m_{\tilde{\tau}_1} \approx m_{\tilde{e}_1, \tilde{\mu}_1}}$ is two times larger than $Y_{\tilde{\tau}}^{m_{\tilde{\tau}_1} \ll m_{\tilde{e}_1, \tilde{\mu}_1}}$ because of selectron/smuon–stau coannihilation processes [15]. In both estimates, the yield $Y_{\tilde{\tau}}$ is proportional to $m_{\tilde{\tau}}$. We have indicated typical uncertainties of the mass bounds with respect to the SUSY model by working with both $Y_{\tilde{\tau}}$ estimates. Another uncertainty is related to the precise value of ϵ_{em} which can also depend on the superparticle spectrum. We have therefore shown bounds obtained with the largest and smallest possible values of ϵ_{em} . Additional constraints from the observed Planck spectrum of the CMB have been updated recently [74]. We find that the new CMB limits reduce the allowed region of $(m_{\tilde{G}}, m_{\tilde{\tau}})$ values only slightly when the conservative BBN bounds are considered. The severe BBN bounds however are more severe than the CMB limits in any region of the $(m_{\tilde{G}}, m_{\tilde{\tau}})$ plane.

We have obtained new mass bounds from our result for ϵ_{had} . By comparing our new bounds with the outdated ones, we find that the previous estimate of ϵ_{had} from Ref. [21] leads to overly restrictive mass bounds. In particular, superWIMP gravitino dark matter scenarios, in which the dark matter density is dominated by gravitinos from charged slepton NLSP decays [17, 18, 21], were believed to be excluded by the severe BBN bounds [22]. With our update of the constraints from hadronic energy release, we find that such scenarios will still be viable at $(m_{\tilde{G}}, m_{\tilde{\tau}}) = (200 \text{ GeV}, 2.8 \text{ TeV})$ for $m_{\tilde{\tau}_1} \ll m_{\tilde{e}_1, \tilde{\mu}_1}$ or $(m_{\tilde{G}}, m_{\tilde{\tau}}) = (120 \text{ GeV}, 2.2 \text{ TeV})$ for $m_{\tilde{\tau}_1} \approx m_{\tilde{e}_1, \tilde{\mu}_1}$, even if the severe BBN bounds are valid. With the conservative BBN bounds, superWIMP scenarios are also viable around $(m_{\tilde{G}}, m_{\tilde{\tau}}) = (450 \text{ GeV}, 1.2 \text{ TeV})$ for $m_{\tilde{\tau}_1} \ll m_{\tilde{e}_1, \tilde{\mu}_1}$ or $(m_{\tilde{G}}, m_{\tilde{\tau}}) = (280 \text{ GeV}, 1 \text{ TeV})$ for $m_{\tilde{\tau}_1} \approx m_{\tilde{e}_1, \tilde{\mu}_1}$.

From the cosmological constraints, we find an upper limit on the mass of the gravitino LSP of (100 – 700) GeV in scenarios with a charged slepton NLSP. The wide range is due to the aforementioned uncertainties. We have outlined potential insights from future experiments that can help to reduce these uncertainties.

In addition to scenarios in which the NLSP sleptons freeze out with a thermal abundance, we have also considered scenarios in which a given fraction f of $\Omega_{\text{CDM}}^{\text{obs}}$ comprises of gravitinos from NLSP decays. The electromagnetic and hadronic nucleosynthesis constraints on $m_{\tilde{G}}$ and $m_{\tilde{\tau}}$ have been given for $f = 1, 0.1,$ and 0.01 . The constraint from $\Omega_{\text{CDM}}^{\text{obs}}$ is respected in such scenarios by definition. Since we consider the thermal NLSP abundance as the natural one, we have indicated explicitly the range in which the NLSP yield $Y_{\tilde{\tau}}$ required for $\Omega_{\tilde{G}}^{\text{NTP}} = f \Omega_{\text{CDM}}^{\text{obs}}$ agrees with the estimates $Y_{\tilde{\tau}}^{m_{\tilde{\tau}_1} \ll m_{\tilde{e}_1, \tilde{\mu}_1}}$ and $Y_{\tilde{\tau}}^{m_{\tilde{\tau}_1} \approx m_{\tilde{e}_1, \tilde{\mu}_1}}$.

In our study of the relic gravitino density from thermal production, $\Omega_{\tilde{G}}^{\text{TP}}$, we have used the gauge-invariant result of Ref. [16]. While the final result for $\Omega_{\tilde{G}}^{\text{TP}}$ was only given in the limit $m_{\tilde{G}} \ll m_{\tilde{g}}$ in Ref. [16], we have presented results obtained from the more general expression valid also for $m_{\tilde{G}} \approx m_{\tilde{g}}$ [25]. We have shown explicitly that the contribution from the spin-3/2 components of the gravitino becomes important for $m_{\tilde{G}} \gtrsim 0.5 m_{\tilde{g}}$.

The dependence of $\Omega_{\tilde{G}}^{\text{TP}}$ on the reheating temperature after inflation T_R has allowed us to provide upper limits on T_R for scenarios in which a given fraction $(1 - f)$ of $\Omega_{\text{CDM}}^{\text{obs}}$ comprises of thermally produced gravitinos. We have described how these limits can be tightened by constraints from late slepton NLSP decays. Implications of the T_R limits have been discussed for successful thermal leptogenesis which requires $T_R \gtrsim 3 \times 10^9$ GeV [48]. While thermal leptogenesis cannot explain the baryon asymmetry in superWIMP gravitino dark matter scenarios with $\Omega_{\text{CDM}}^{\text{obs}} \approx \Omega_{\tilde{G}}^{\text{NTP}}$, we find that the required reheating temperatures become allowed for $m_{\tilde{G}} \gtrsim 50$ GeV and $m_{\tilde{g}} \lesssim 1$ TeV in scenarios with $\Omega_{\text{CDM}}^{\text{obs}} \approx \Omega_{\tilde{G}}^{\text{TP}}$.

We have computed the present free-streaming velocity of gravitinos from thermal production and of gravitinos from NLSP decays. We find that thermally produced gravitinos with $m_{\tilde{G}} \gtrsim 100$ keV can be classified as cold dark matter since they have a negligible free-streaming velocity today. In contrast, gravitinos from late decays of a charged slepton NLSP can be classified as warm dark matter in large regions of the parameter space [13, 58, 59, 27]. We have listed upper limits on the present free-streaming velocities from simulations and observations of cosmic structures. For superWIMP gravitino dark matter scenarios with $\Omega_{\text{CDM}}^{\text{obs}} \approx \Omega_{\tilde{G}}^{\text{NTP}}$, we find that these upper limits exclude slepton NLSPs with a mass of $m_{\tilde{\tau}} \lesssim 0.5$ TeV, and even $m_{\tilde{\tau}}$ values up to about 1 TeV could be excluded with a better understanding of cosmological reionization and the Next Generation Space Telescope. However, natural superWIMP gravitino dark matter scenarios require anyhow $m_{\tilde{\tau}} \gtrsim 1$ TeV. As warm dark matter, the superWIMP gravitinos could explain the matter power spectrum on small scales, which is significantly lower than expected from N-body simulations of cold dark matter [58, 59].

For gravitino LSP scenarios with a charged slepton NLSP, we have outlined the possible interplay between astrophysical investigations and studies at future colliders. If not too heavy, charged NLSP sleptons will appear as long-lived charged particles in planned collider detectors. Such signals would point to an extremely weakly interacting LSP and could allow one to measure $m_{\tilde{\tau}}$ [41]. Assuming the gravitino LSP scenario, this $m_{\tilde{\tau}}$ value can be used to refine the upper bound on $m_{\tilde{G}}$ from the cosmological constraints presented in this paper. If, in addition, the lifetime of the NLSP, $\tau_{\tilde{\tau}}$, can be measured, one will be able to determine the mass of a possible gravitino LSP from the SUGRA prediction for $\tau_{\tilde{\tau}}$ [41, 42]. We have

emphasized that an experimental determination of $(m_{\tilde{G}}, m_{\tilde{\tau}})$ would impose upper limits on the gravitino density from NLSP decays, $\Omega_{\tilde{G}}^{\text{NTP}}$, and thereby improve the upper limit on the reheating temperature after inflation T_R .

We have described the possible identification of the gravitino as the LSP at future colliders. With an analysis of the NLSP decays in massive additional material around planned collider detectors [43, 44], distinguishing the gravitino LSP from the axino LSP could be possible [45, 25]. Moreover, with a kinematical determination of the LSP mass and the measured values for $m_{\tilde{\tau}}$ and $\tau_{\tilde{\tau}}$, one can extract the Planck scale M_{Pl} from the SUGRA prediction for $\tau_{\tilde{\tau}}$. An agreement with macroscopic measurements of M_{Pl} would be strong evidence for the existence of the gravitino LSP [42].

The various insights gained from the cosmological constraints and the prospects for collider phenomenology have been summarized in terms of ten viable benchmark scenarios with a gravitino LSP and a stau NLSP. We find three groups of scenarios:

- (i) Warm (superWIMP) gravitino dark matter from stau NLSP decays, $\Omega_{\text{CDM}}^{\text{obs}} \approx \Omega_{\tilde{G}}^{\text{NTP}}$. These scenarios could resolve the small scale structure problems of cold dark matter but are associated with severe limits on T_R and a stau NLSP with a mass of $m_{\tilde{\tau}} \gtrsim 1$ TeV, which will be difficult to produce at the LHC.
- (ii) Mixed cold/warm gravitino dark matter with considerable contributions from thermal production and stau NLSP decays. In these scenarios, the very high reheating temperature of $T_R \gtrsim 3 \times 10^9$ GeV needed for successful thermal leptogenesis is possible. The mass of the stau NLSP in these scenarios is typically $m_{\tilde{\tau}} \gtrsim 0.7$ TeV so that it could still be discovered at the LHC.
- (iii) Cold gravitino dark matter from thermal production, $\Omega_{\text{CDM}}^{\text{obs}} \approx \Omega_{\tilde{G}}^{\text{TP}}$. In these scenarios, very high reheating temperatures of $T_R \gtrsim 10^9$ GeV can still be allowed. Since the mass of the stau NLSP can be as small as 100 GeV, these scenarios are very promising for collider phenomenology and could be accessible even at the ILC.

It remains to be seen if any of these scenarios can be verified in future experiments. In view of the upcoming collider experiments at the LHC, it will be worthwhile to further refine the cosmological constraints presented in this work.

Acknowledgements

I am grateful to A. Brandenburg, W. Buchmüller, L. Covi, M. Drees, B. Eberle, T. Hahn, K. Hamaguchi, W. Kilian, M. Maniatis, T. Plehn, M. Plümacher, J. Pradler, G. Raffelt, J. Reuter, T. Robens, P. D. Serpico, Y.Y.Y. Wong, and P. Zerwas for valuable discussions. I also thank J. Kersten for bringing several typographical errors to my attention.

References

- [1] H. P. Nilles, Phys. Rep. **110** (1984) 1;
H. E. Haber and G. L. Kane, Phys. Rep. **117** (1985) 75;
S. P. Martin, *A supersymmetry primer*, hep-ph/9709356.

- [2] J. Wess and J. Bagger, *Supersymmetry and supergravity* (Princeton University Press, Princeton, 1992).
- [3] M. Dine, A. E. Nelson, and Y. Shirman, Phys. Rev. D **51** (1995) 1362 [hep-ph/9408384];
M. Dine, A. E. Nelson, Y. Nir, and Y. Shirman, Phys. Rev. D **53** (1996) 2658 [hep-ph/9507378];
G. F. Giudice and R. Rattazzi, Phys. Rep. **322** (1999) 419 [hep-ph/9801271].
- [4] L. Randall and R. Sundrum, Nucl. Phys. B **557** (1999) 79 [hep-th/9810155];
G. F. Giudice, M. A. Luty, H. Murayama, and R. Rattazzi, JHEP **9812** (1998) 027 [hep-ph/9810442].
- [5] W. Buchmüller, K. Hamaguchi, and J. Kersten, Phys. Lett. B **632** (2006) 366 [hep-ph/0506105].
- [6] E. Cremmer, S. Ferrara, L. Girardello, and A. Van Proeyen, Nucl. Phys. B **212** (1983) 413.
- [7] S. Eidelman *et al.* [Particle Data Group], Phys. Lett. B **592** (2004) 1.
- [8] H. Pagels and J. R. Primack, Phys. Rev. Lett. **48** (1982) 223.
- [9] J. R. Ellis, D. V. Nanopoulos, and S. Sarkar, Nucl. Phys. B **259** (1985) 175.
- [10] V. S. Berezinsky, Phys. Lett. B **261** (1991) 71.
- [11] T. Moroi, H. Murayama, and M. Yamaguchi, Phys. Lett. B **303** (1993) 289.
- [12] J. R. Ellis, D. V. Nanopoulos, K. A. Olive, and S. J. Rey, Astropart. Phys. **4** (1996) 371 [hep-ph/9505438].
- [13] S. Borgani, A. Masiero, and M. Yamaguchi, Phys. Lett. B **386** (1996) 189 [hep-ph/9605222].
- [14] M. Bolz, W. Buchmüller, and M. Plümacher, Phys. Lett. B **443** (1998) 209 [hep-ph/9809381].
- [15] T. Asaka, K. Hamaguchi, and K. Suzuki, Phys. Lett. B **490** (2000) 136 [hep-ph/0005136].
- [16] M. Bolz, A. Brandenburg, and W. Buchmüller, Nucl. Phys. B **606** (2001) 518 [hep-ph/0012052].
- [17] J. L. Feng, A. Rajaraman, and F. Takayama, Phys. Rev. Lett. **91** (2003) 011302 [hep-ph/0302215].
- [18] J. L. Feng, A. Rajaraman, and F. Takayama, Phys. Rev. D **68** (2003) 063504 [hep-ph/0306024].
- [19] M. Fujii, M. Ibe, and T. Yanagida, Phys. Lett. B **579** (2004) 6 [hep-ph/0310142].
- [20] J. R. Ellis, K. A. Olive, Y. Santoso, and V. C. Spanos, Phys. Lett. B **588** (2004) 7 [hep-ph/0312262].
- [21] J. L. Feng, S. Su, and F. Takayama, Phys. Rev. D **70** (2004) 063514 [hep-ph/0404198].
- [22] J. L. Feng, S. Su, and F. Takayama, Phys. Rev. D **70** (2004) 075019 [hep-ph/0404231].
- [23] L. Roszkowski, R. Ruiz de Austri, and K. Y. Choi, JHEP **0508** (2005) 080 [hep-ph/0408227];
D. G. Cerdeno, K. Y. Choi, K. Jedamzik, L. Roszkowski and R. Ruiz de Austri, JCAP **0606** (2006) 005 [arXiv:hep-ph/0509275].

- [24] K. Jedamzik, M. Lemoine and G. Moulataka, Phys. Rev. D **73** (2006) 043514 [hep-ph/0506129];
M. Lemoine, G. Moulataka and K. Jedamzik, *Natural gravitino dark matter in $SO(10)$ gauge mediated supersymmetry breaking*, hep-ph/0504021.
- [25] F. D. Steffen, *Collider signatures of axino and gravitino dark matter*, hep-ph/0507003.
- [26] A. L. Maroto and A. Mazumdar, Phys. Rev. Lett. **84** (2000) 1655 [hep-ph/9904206];
R. Kallosh, L. Kofman, A. D. Linde, and A. Van Proeyen, Phys. Rev. D **61** (2000) 103503 [hep-th/9907124];
G. F. Giudice, A. Riotto, and I. Tkachev, JHEP **9911** (1999) 036 [hep-ph/9911302];
R. Allahverdi, M. Bastero-Gil and A. Mazumdar, Phys. Rev. D **64** (2001) 023516 [hep-ph/0012057];
H. P. Nilles, M. Peloso, and L. Sorbo, Phys. Rev. Lett. **87** (2001) 051302 [hep-ph/0102264].
- [27] K. Jedamzik, M. Lemoine and G. Moulataka, JCAP **0607** (2006) 010 [astro-ph/0508141].
- [28] M. Kawasaki, K. Kohri, and T. Moroi, Phys. Lett. B **625** (2005) 7 [astro-ph/0402490].
- [29] M. Kawasaki, K. Kohri, and T. Moroi, Phys. Rev. D **71** (2005) 083502 [astro-ph/0408426].
- [30] E. Holtmann, M. Kawasaki, K. Kohri, and T. Moroi, Phys. Rev. D **60** (1999) 023506 [hep-ph/9805405].
- [31] R. H. Cyburt, J. R. Ellis, B. D. Fields, and K. A. Olive, Phys. Rev. D **67** (2003) 103521 [astro-ph/0211258].
- [32] M. H. Reno and D. Seckel, Phys. Rev. D **37** (1988) 3441.
- [33] S. Dimopoulos, R. Esmailzadeh, L. J. Hall, and G. D. Starkman, Astrophys. J. **330** (1988) 545; Nucl. Phys. B **311** (1989) 699.
- [34] K. Kohri, Phys. Rev. D **64** (2001) 043515 [astro-ph/0103411].
- [35] K. Jedamzik, Phys. Rev. D **70** (2004) 063524 [astro-ph/0402344].
- [36] M. Drees and X. Tata, Phys. Lett. B **252** (1990) 695.
- [37] A. Nisati, S. Petrarca, and G. Salvini, Mod. Phys. Lett. A **12** (1997) 2213 [hep-ph/9707376].
- [38] S. Ambrosanio, G. D. Kribs, and S. P. Martin, Phys. Rev. D **56** (1997) 1761 [hep-ph/9703211].
- [39] J. L. Feng and T. Moroi, Phys. Rev. D **58** (1998) 035001 [hep-ph/9712499].
- [40] S. P. Martin and J. D. Wells, Phys. Rev. D **59** (1999) 035008 [hep-ph/9805289].
- [41] S. Ambrosanio, B. Mele, S. Petrarca, G. Polesello, and A. Rimoldi, JHEP **0101** (2001) 014 [hep-ph/0010081].
- [42] W. Buchmüller, K. Hamaguchi, M. Ratz, and T. Yanagida, Phys. Lett. B **588** (2004) 90 [hep-ph/0402179]; *Gravitino and goldstino at colliders*, hep-ph/0403203.
- [43] K. Hamaguchi, Y. Kuno, T. Nakaya, and M. M. Nojiri, Phys. Rev. D **70** (2004) 115007 [hep-ph/0409248].
- [44] J. L. Feng and B. T. Smith, Phys. Rev. D **71** (2005) 015004 [hep-ph/0409278].
- [45] A. Brandenburg, L. Covi, K. Hamaguchi, L. Roszkowski, and F. D. Steffen, Phys. Lett. B **617** (2005) 99 [hep-ph/0501287].

- [46] A. De Roeck *et al.*, *Supersymmetric benchmarks with non-universal scalar masses or gravitino dark matter*, hep-ph/0508198.
- [47] M. Fukugita and T. Yanagida, Phys. Lett. B **174** (1986) 45.
- [48] W. Buchmüller, P. Di Bari, and M. Plümacher, Annals Phys. **315** (2005) 305 [hep-ph/0401240].
- [49] J. Gratsias, R. J. Scherrer, and D. N. Spergel, Phys. Lett. B **262** (1991) 298.
- [50] M. Kawasaki and T. Moroi, Phys. Lett. B **346** (1995) 27 [hep-ph/9408321].
- [51] K. Kohri, T. Moroi and A. Yotsuyanagi, Phys. Rev. D **73** (2006) 123511 [hep-ph/0507245].
- [52] D. N. Spergel *et al.*, Astrophys. J. Suppl. **148** (2003) 175. [astro-ph/0302209].
- [53] B. D. Fields and K. A. Olive, Astrophys. J. **506** (1998) 177 [astro-ph/9803297].
- [54] Y. I. Izotov and T. X. Thuan, Astrophys. J. **602** (2004) 200 [astro-ph/0310421].
- [55] LEPSUSYWG, ALEPH, DELPHI, L3, and OPAL experiments, note LEPSUSYWG/02-05.1; see also note LEPSUSYWG/02-09.2 (<http://lepsusy.web.cern.ch/lepsusy/Welcome.html>).
- [56] D. N. Spergel *et al.*, *Wilkinson Microwave Anisotropy Probe (WMAP) three year results: Implications for cosmology*, astro-ph/0603449.
- [57] E. W. Kolb and M. S. Turner, *The Early Universe* (Addison-Wesley, Redwood City, 1990).
- [58] M. Kaplinghat, Phys. Rev. D **72** (2005) 063510 [astro-ph/0507300].
- [59] J. A. R. Cembranos, J. L. Feng, A. Rajaraman, and F. Takayama, Phys. Rev. Lett. **95** (2005) 181301 [hep-ph/0507150].
- [60] W. B. Lin, D. H. Huang, X. Zhang, and R. H. Brandenberger, Phys. Rev. Lett. **86** (2001) 954 [astro-ph/0009003].
- [61] J. Hisano, K. Kohri, and M. M. Nojiri, Phys. Lett. B **505** (2001) 169 [hep-ph/0011216].
- [62] P. Bode, J. P. Ostriker, and N. Turok, Astrophys. J. **556** (2001) 93 [astro-ph/0010389].
- [63] J. J. Dalcanton and C. J. Hogan, Astrophys. J. **561** (2001) 35 [astro-ph/0004381].
- [64] V. K. Narayanan, D. N. Spergel, R. Dave, and C. P. Ma, Astrophys. J. **543** (2000) L103 [astro-ph/0005095].
- [65] M. Viel, J. Lesgourgues, M. G. Haehnelt, S. Matarrese, and A. Riotto, Phys. Rev. D **71** (2005) 063534 [astro-ph/0501562].
- [66] R. Barkana, Z. Haiman, and J. P. Ostriker, Astrophys. J. **558** (2001) 482 [astro-ph/0102304].
- [67] L. Page *et al.*, *Three year Wilkinson Microwave Anisotropy Probe (WMAP) observations: Polarization analysis*, astro-ph/0603450.
- [68] N. Yoshida, A. Sokasian, L. Hernquist, and V. Springel, Astrophys. J. **591** (2003) L1 [astro-ph/0303622].
- [69] P. Colin, V. Avila-Reese, and O. Valenzuela, Astrophys. J. **542** (2000) 622 [astro-ph/0004115].
- [70] K. Sigurdson and M. Kamionkowski, Phys. Rev. Lett. **92**, 171302 (2004) [astro-ph/0311486].
- [71] T. Gherghetta, G. F. Giudice, and A. Riotto, Phys. Lett. B **446** (1999) 28 [hep-ph/9808401].

- [72] P. Gondolo *et al.*, JCAP **0407** (2004) 008 [astro-ph/0406204].
- [73] G. Belanger, F. Boudjema, A. Pukhov, and A. Semenov, Comput. Phys. Commun. **149** (2002) 103 [hep-ph/0112278]; *ibid.* **174** (2006) 577 [hep-ph/0405253].
- [74] R. Lamon and R. Dürrer, Phys. Rev. D **73** (2006) 023507 [hep-ph/0506229].
- [75] D. J. Fixsen *et al.*, Astrophys. J. **473** (1996) 576 [astro-ph/9605054].
- [76] W. Hu and J. Silk, Phys. Rev. D **48** (1993) 485.
- [77] E. Braaten and T. C. Yuan, Phys. Rev. Lett. **66** (1991) 2183.
- [78] E. Braaten and R. D. Pisarski, Nucl. Phys. B **337** (1990) 569.
- [79] J. L. Goity, W. J. Kossler, and M. Sher, Phys. Rev. D **48** (1993) 5437 [hep-ph/9305244].
- [80] L. Covi, L. Roszkowski, R. Ruiz de Austri, and M. Small, JHEP **0406** (2004) 003. [hep-ph/0402240].
- [81] L. Covi, H. B. Kim, J. E. Kim, and L. Roszkowski, JHEP **0105** (2001) 033 [hep-ph/0101009].
- [82] A. Brandenburg and F. D. Steffen, JCAP **0408** (2004) 008 [hep-ph/0405158]; *Axinos as dark matter in the Universe*, hep-ph/0406021; *Thermal production of axinos in the early Universe*, hep-ph/0407324.
- [83] A. Kudo and M. Yamaguchi, Phys. Lett. B **516** (2001) 151 [hep-ph/0103272].
- [84] J. Preskill, M. B. Wise, and F. Wilczek, Phys. Lett. B **120** (1983) 127;
L. F. Abbott and P. Sikivie, Phys. Lett. B **120** (1983) 133;
M. Dine and W. Fischler, Phys. Lett. B **120** (1983) 137.